The Multichromatic Wavelet Transformation as a Source Identification Tool for GLAST

Sean M. Robinson

A dissertation submitted in partial fulfillment of the requirements for the degree of

Doctor of Philosophy

University of Washington

2004

Program Authorized to Offer Degree:
Department of Physics

University of Washington
Graduate School

This is to certify that I have examined this copy of a doctoral dissertation by

Sean M. Robinson

and have found that it is complete and satisfactory in all respects, and that any and all revisions required by the final examining committee have been made.

Chair of Supervisory Committee:

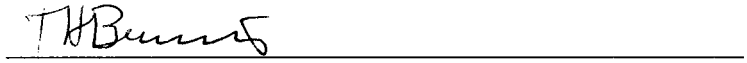

Toby Burnett

Reading Committee:

Toby Burnett

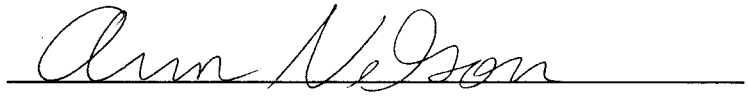

Ann Nelson

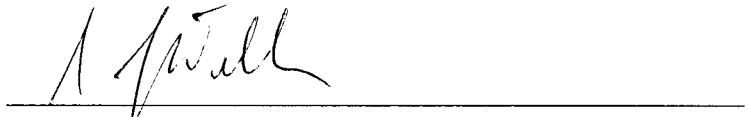

Jeffrey Wilkes

Date Aug. 16, 2004

In presenting this dissertation in partial fulfillment of the requirements for the doctoral degree at the University of Washington, I agree that the Library shall make its copies freely available for inspection. I further agree that extensive copying of the dissertation is allowable only for scholarly purposes, consistent with .fair use. as prescribed in the U.S. Copyright Law. Requests for copying or reproduction of this dissertation may be referred to Proquest Information and Learning, 300 North Zeeb Road, Ann Arbor, MI 48106-1346, to whom the author has granted "the right to reproduce and sell (a) copies of the manuscript in microform and/or (b) printed copies of the manuscript made from microform."

Signature Aug. 16, 2004

Date

University of Washington

Abstract

The Multichromatic Wavelet Transformation as a Source Identification Tool for GLAST

Sean M. Robinson

Chair of the Supervisory Committee:
Professor Toby Burnett
Physics Department

The GLAST mission (Gamma-ray Large Area Space Telescope) will yield a great amount of photon data in the region from 30 MeV to 300 GeV. However, the sparsity of incoming photon events and strong dependence of instrument response on photon energy necessitate data analysis techniques different from those used in similar areas such as X-Ray astronomy. A modified form of the continuous wavelet transformation (CWT) has been developed for use in finding point sources from sparse photon data. This method has multiple advantages over other source location strategies, and is developed as a source finding algorithm. As the efficiency of this method is well characterized, this method is also useful in estimation of the total contribution of unresolvable sources to the observed extragalactic gamma-ray intensity. Using this method, we are able to estimate the ratio of the extragalactic gamma-ray background accounted for by diffuse emission of photons. With foreknowledge of the instrument response of GLAST, and the point-source resolution algorithm to be used, an estimate can be made of the diffuse component necessary to be significantly measured in this

way. This "diffuse discrimination threshold" has been measured for GLAST, at the level of a few percent. The Point Soure Sensitivity (PSS) of GLAST has also been estimated to be about $7.0 \cdot 10^{-9}$ $cm^{-2}s^{-1}$.

Table of Contents

List of Figures

Glossary

Generally:

$\mathbf{r}$ - a Position Vector
E - Energy
i - Index Identifying a Given Datum (Photon Event)
$\mathbf{r}_i$, E_i, etc. - Characteristics of Photon i.

When Describing a Single Point Source:

N - Source Counts
r - Source Rate (Counts/Second)
S - Source Density (Counts/$Second \cdot cm^2$)
$\mathbf{b}$ - Source Location
θ - Angular Distance (Measured From the Source)
B - Background Counts
b - Background Density (Counts/Second·cm^2·Steradian)
r_b - Relative Background Density (b/S in the direction of the source)

Relating to the Wavelet Transformation:

W - Wavelet Transformation
I - Photon Data
ψ - Analyzing Wavelet Function
α - The Dilation Factor
a - The Dilation Coefficient

Acknowledgements

The author would like to acknowledge many people for their continued support in this and other projects, most notably including his parents and family for their unconditional encouragement and love, the Physics Department at the University of Washington for being a challenging and supportive environment, and professor Toby Burnett for providing excellent guidance, assistance, and mentorship. Furthermore, without the support, and occasional critique from my friends and colleagues, this work would not have been possible.

Chapter 1

Introduction

Observations of the celestial photon emission have chiefly resolved gamma-ray luminous objects in the form of AGN's (Active Galactic Nuclei) and pulsars. Aside from such "point" sources, a diffuse, spatially anisotropic emission has been observed, believed to be galactic in origin, and largely due to the interaction between cosmic rays and interstellar matter, and also inverse-compton scattering of high-energy cosmic rays on intragalactic photons. There is also an observed, isotropic component to the gamma-ray sky (Sreekumar et.al , 1998), more visible at high galactic latitude where the former mechanisms of emission account for less flux. It has been suggested (Stecker & Salamon, 1996) that the Extragalactic diffuse gamma-ray emission arises from the sum of distant AGN sources that are simply unresolved (i.e. unresolvable from current data sets.) Though the current catalog of known gamma-ray emissive sources does not contradict this possibility, the low number of resolved objects (on the order of 100) would, in principle, allow for a large percentage of the remaining "unclaimed" extragalactic flux to have a truly diffuse origin, such as the photon emissions from cosmic rays interacting with intergalactic matter. Herein, we develop an

analysis method to estimate a lower limit to the "truly diffuse" component of the EDGRB (Extragalactic Diffuse Gamma-ray Background), as well as analytic results developing limits on source resolvability and distribution. Firstly, given a model for the extragalactic emission (point sources corresponding to a logN/logS characteristic and an isotropic diffuse component), we would like to know how many sources a particular experiment could hope to resolve, and in what distribution. Secondly, we would like to know how this "resolved distribution" will change with the proportion of extragalactic emission due to truly diffuse mechanisms. This should allow an experimental limit on diffuse emission to be set with respect to a particular experiment. In other words, above a certain threshold of diffuse intensity, a given experiment (say GLAST or EGRET) should be able to tell the difference between unresolved point sources and truly diffuse emission. This research should give a threshold to the percentage of emission which "could be diffuse", thanks to the EGRET experiment, and also a threshold percentage above which the GLAST experiment should be able to differentiate between summed point sources and diffuse emission. There will also be a treatment of various source-resolution methods to estimate source locations, energy spectra and intensity from raw observation data. It is a further goal of this research to establish a numerical algorithm in order to accomplish these preceding ends, in which only actual data and knowledge of the experiment used to collect it will allow for estimation of the aforementioned diffuse threshold and source distribution.

Chapter 2

Background Construction

2.1 Model of Blazar Emission

An "active" galaxy is one in which the central area is highly emissive. This is commonly modeled as being due to the presence of a black hole accreting matter at the center of the galaxy. There are also also relativistic jets of matter ejecting in opposite directions, emitting gamma radiation (Fig. 2.1). This mass ejection has been modeled as being due to the magnetohydrodynamic process in the accretion disc. (Tsiklauri & Nakariakov, 2002). Emissions from AGN, extending from soft x-rays into the TeV range, are most often explained by synchrotron and inverse-compton processes within the AGN jet (Kirk et.al, 1998). In the lower-energy region, high time-variability and a strong polarization of the detected photons make a good case for synchrotron emission within the jet. In blazers emissive up to TeV ranges, this emission falls most often between the UV and soft X-ray spectra. The higher peak is less well-understood, and described by both leptonic and hadronic models, referring to electrons and protons, respectively, as being the primary carriers of energy within the jet, responsible for radiation (Rachen, 1999; Sambruna, 1999). In the "leptonic"

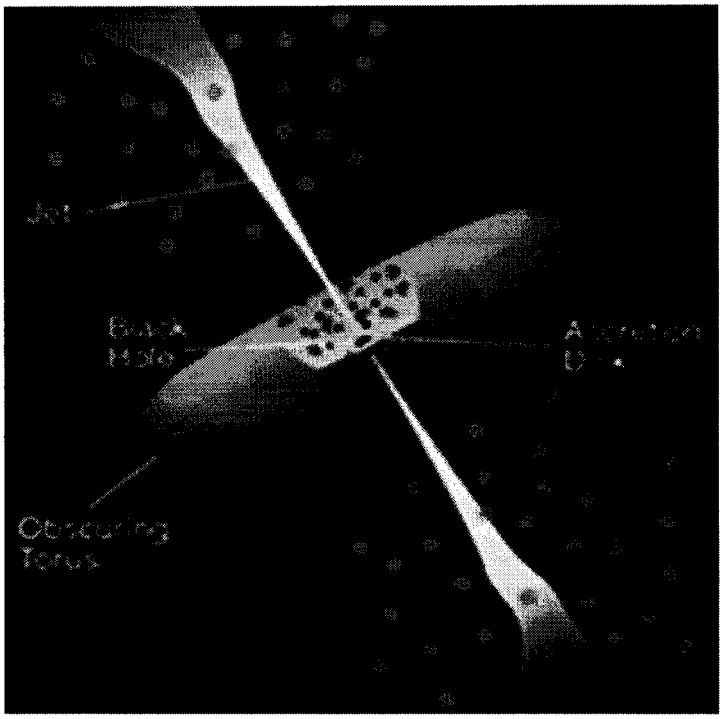

Figure 2.1: Schematic of an AGN

model, high-energy gamma rays are produced primarily from inverse-compton scattering off of the electrons in the jet. The photons scattered are either internal to (Synchrotron Self-Compton, SSC) or external to (External Compton, EC) the jet itself. In the hadronic model(s), protons carry the majority of the energy available for radiation, and photon-proton interactions create either electron-positron pairs, or pions, which later decay into charged pairs. It is these charged-lepton pairs, then, that are responsible for generating gamma-rays through the same processes of the lepton model.

A blazar, likewise, is an AGN whose relativistic jet is pointed in the observer's direction, increasing the emission from the galaxy in the gamma-ray region. In or-

der to numerically simulate the summed emission from many unknown AGN sources, we must first construct a concise model approximating single AGN emission, as well as defining parameters containing the relevant information determining the emissive behavior of a single source. In this way, we must first construct the "random extra-galactic point source" in order to consider the sum of such unknown sources. This said, we begin by studying the known blazar emissions, from a phenomenological perspective.

2.1.1 Phenomenological Blazar Energy Spectrum

It is first important to mention that blazar emissions are normally modeled as having two emissive states - flaring and quiescent. An extremely rough estimate might be that the total luminosity from the source from 20MeV to 300 GeV may be a factor of 5 higher during the flaring state, while the source may be flaring only around a few percent of the total observing time. It is also noted that the energy spectrum hardens during the flaring state (Stecker & Salamon, 1996; Boettcher,Chiang, 2002). As above, energy spectra are generally accepted to have two components - the synchrotron component from the accretion disc, extending from radio frequencies into soft X-rays, and a harder component from inverse-compton scattering, extending from hard X-rays up to TeV energies(Fig. 2.2). The low-energy emissions drive gamma-ray emissions in this model, as the synchroton photons from the lower energy range become gamma rays after inverse-compton scattering. This model has been used widely to explain the observed energy spectra (Kino et.al, 2002; Jones et.al, 1974).

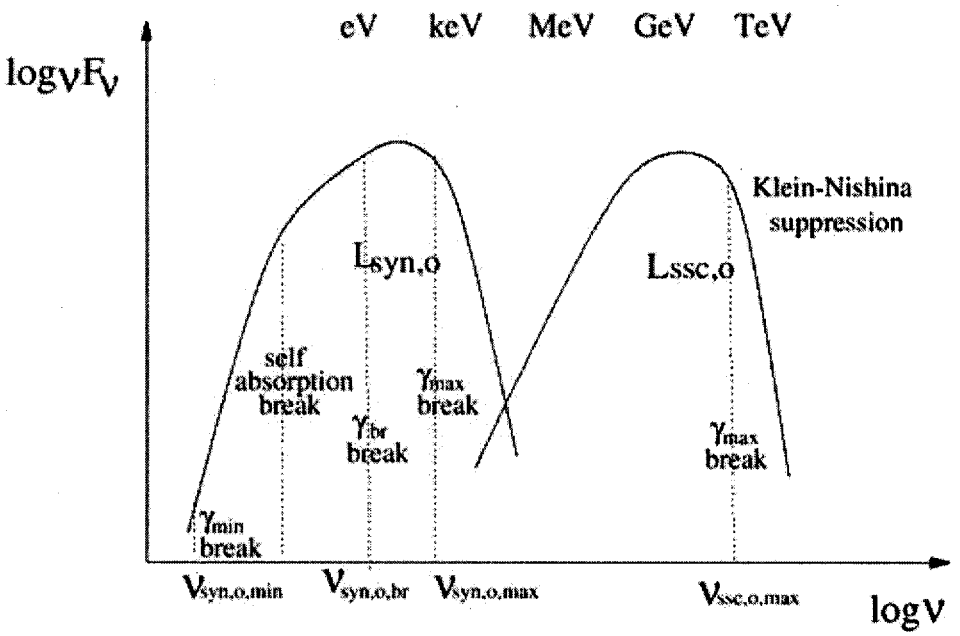

Figure 2.2: Picture of the multi-frequency spectrum of a typical TeV blazar. (Diagram from (Kino et.al, 2002))

2.1.2 Time Variability of Blazars

Blazars exhibit time variability in the x-ray and gamma-ray spectra. In the x-ray case, this variability is well-characterized, and AGN sources exhibit time variability as a rough power law with respect to the periodicity of variation(Nandra, 2000). In the case of the gamma-ray emission, low numbers of candidate sources as well as low total intensities limit our ability to characterize the flaring characteristics of the AGN population. Even so, there is clear evidence for AGN flaring in the gamma ray region, and some estimates have been made as to the strength and timescale of these variations (Stecker & Salamon, 1996).

2.2 The Cosmological Model & logN/logS

2.2.1 Spatial Isotropy of Sources

It is assumed that the density of blazars is spatially isotropic. It is important to note that, though this is only allowed due to further assumptions about universal structure, it is fair to allow within a calculation about AGN emission. As the density of sources is an unknown parameter, the probability density of point sources at a given angular direction would have to have large variances to cause a statistically significant deviation in the observed density of sources. Spatial anisotropy in point source distribution, even at the level of a few percent, though interesting, should not perturb the result of this research by any significant amount. However, the homogeneity assumption cannot be taken as strictly correct, thanks to the unlikeliness

of gamma-ray sources in the very early universe. Thus, at some redshift, the relative number density of emissive sources must fall off, and studies have been undertaken to model this falloff in the x-ray region (Nemiroff e.al, 1995; Stecker & Salamon, 1996; Chiang ,Mukherjee, 1998).

2.2.2 Sources of Galactic Diffuse Emission

At redshifts less than about 1000 (after matter decoupling in the universe), the Cosmic Microwave Background (CMB) has been perturbed by a number of influences. Among these is "Comptonisation," the effect of the remaining hot gas of charged particles upon the CMB. The effectiveness of the energy transfer between the hot electrons and the CMB is largely governed by the Sunyaev-Zel'dovich parameter:

$$y \approx \frac{k_B T_e}{m_e c^2} \tau_T \tag{2.1}$$

which describes the difference in temperature between the electrons and the radiation (Lachieze-Rey & Gunzig, 1999, p.111). Current observations (APS, 2002) tend to show that

$$y \leq 1.5 * 10^{-5} \tag{2.2}$$

Thus, as the corresponding distortion to the effective temperature of the CMB spectrum is:

$$\frac{\partial T}{T} = y\left(x\frac{e^x+1}{e^x-1} - 4\right), \text{where } x = \frac{h\nu}{k_B T_\gamma} \tag{2.3}$$

and the spectral density of photons at high frequency (Wien's approximation) gives:

$$u(\nu) \approx 8\pi h\nu^3 c^{-3} exp\left(\frac{-h\nu}{k_B T}\right) \tag{2.4}$$

we can quickly extrapolate that the estimated density of photons in the GeV range due to comptonization will be vanishingly small. However, the case has been made (Dar,Shaviv, 1995) that interactions of cosmic rays with extragalactic gas could account for a large proportion of the observed background. Furthermore, it has been estimated that the sum of distant point sources could account for the entire observed flux (Stecker,Salamon, 1996), and also that it could account for a much smaller fraction (Chiang et.al, 1995). With this in mind, we note that the contribution of various source models to the observed extragalactic intensity above 100 MeV is a contested issue at this time.

2.3 logN/logS

If the universe is spatially isotropic, then we could assume that the density of extragalactic sources at any distance would be constant, up to the cosmological falloff of source density mentioned in section 2.2.1. With such a model, we could attempt to graph the number of sources within a given observed intensity bin, against that intensity. In this "uniform universe" model, we would expect to see the plot of "log(N) vs.

log(S)" (where N is the number of sources and S is the integral flux) to be a straight line, as the average observed intensity of a source would vary as r^{-2}, and the volume of space per unit distance varies as r^3. Thus, we would expect spatial volume (and thus source number) to go up as r^3, and intensity to go down as r^{-2}, implying a slope to the logN/logs curve of $\frac{-3}{2}$ (See dotted line in Fig. 2.3). However, this assumption cannot be exactly correct, due to the cosmological timescales implied by high-redshift sources. At some point, we must expect a time-threshold, before which no gamma-ray loud sources will be observable, as none will be able to have formed before this in the early universe. For this reason, we expect the logN/logS curve to "fall off" at lower intensities (Fig. 2.3). This curve has been estimated through analysis of the EGRET data to a cutoff of around $10^{-9}\,(\mathrm{cm}^{-2}\mathrm{s}^{-1})$(Stecker & Salamon, 1996).

2.3.1 The Cosmological LogN/LogS Calculation

Although the functional form of LogN/logS is easy to approximate in the regime of high intensity (Fig. 2.3), below some intensity the number of sources must fall off, due to density evolution in the early universe. Below some threshold (and thus, before some time in the early universe), we cannot expect AGN sources to exist. Thus, we expect a density evolution with respect to redshift. Furthermore, we must consider the luminosity evolution of sources. We could fit the luminosity of a source with respect to redshift to be

$$L(z) = L_0(1+z)^{\beta} \tag{2.5}$$

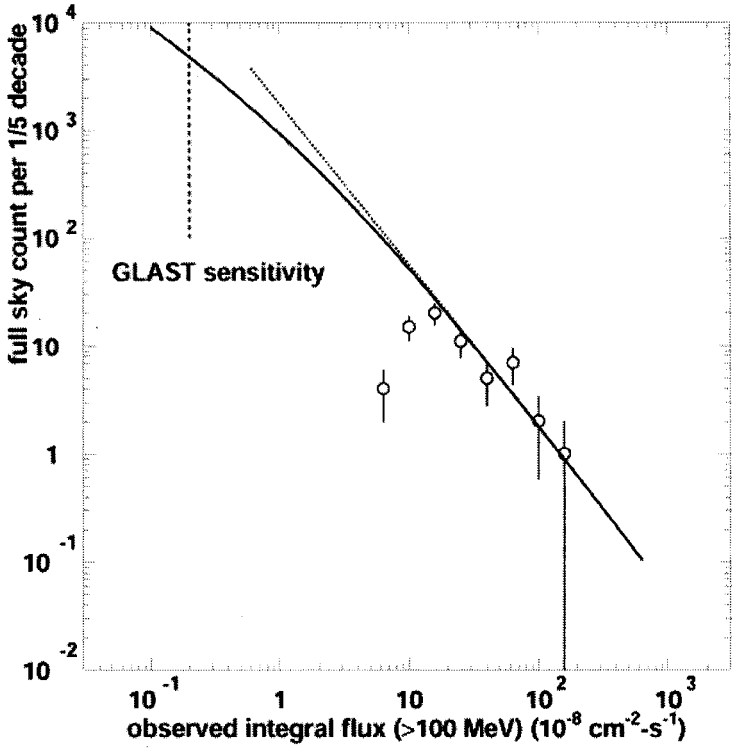

Figure 2.3: logN/logS with tangent and sensitivity cutoffs labelled. Data points are EGRET measurements. Figure from (Stecker & Salamon, 1996)

as done in citepchia95, where z is the redshift of the source, L_0 is the luminosity of the object in the present epoch, and β is a parameter to be fitted. Using this estimate for the luminosity evolution, we could attempt to fit the EGRET data to a logN/logS model, and integrate over the total summed intensity in each bin, giving a contribution of the AGN to the isotropic radiation, as in section 5.5.1. However, the unknown density evolution at high redshift makes a good measure of this difficult, as the great number of dim sources expected determine much of the contribution to the total emission. Possible cumulative intensities (which would determine the contribution of AGN) depend on the density evolution of AGN at high redshift (see Fig. 2.4). Furthermore, as GLAST is sensitive to energies beyond the EGRET instrumental limitation, the luminosity function will need to be examined again. Thus, for the remainder of this work, we will consider a logN/logS curve following that calculated by (Stecker & Salamon, 1996), in which the emissions from unresolved AGN account for all of the extragalactic intensity. As we will see, if there is a nonzero diffuse extragalactic emission component, the catalog of bright sources will need to change accordingly, as developed in the following section.

2.3.2 The Summed Extragalactic Background

With the above results, we will attempt to create a working model of the background as a combination of an isotropic diffuse luminosity overlaid with point sources corresponding to the logN/logS characteristic. The measurement of the total sky emission gives a relationship between the diffuse and point-source flux, as these components

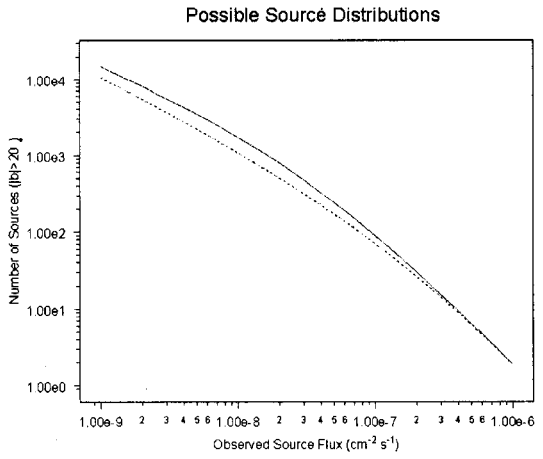

Figure 2.4: Possible logN/logS curves. Solid line is calculated using the redshift/number density evolution curve from (Stecker & Salamon, 1996), dashed line is with the opposite evolution.

must add together to equal the total flux(See Sec. 5.5). So, assuming that the distribution of production of diffuse extragalactic photons is also spatially isotropic (for example, cosmic rays incident upon intergalactic baryons), we can presume that the number of observed sources in a differential intensity range would be proportionally smaller, thanks to the diffuse intensity accounting for some of the emission from that range. For the remainder of this discussion, I will denote the ratio between the truly diffuse EGRB and the total EGRB to be the "ratio of total intensity" 'D'. (See Figure 2.5). D is thus the ratio of the extragalactic isotropic radiation which comes from truly diffuse emission, as opposed to point sources. It is important to note that we have assumed a possible extragalactic diffuse emission which presents negligible time evolution, throughout this work. In the limit of small redshift, and as the mechanism for such emission is unknown, this seems a reasonable assumption. However, if a diffuse

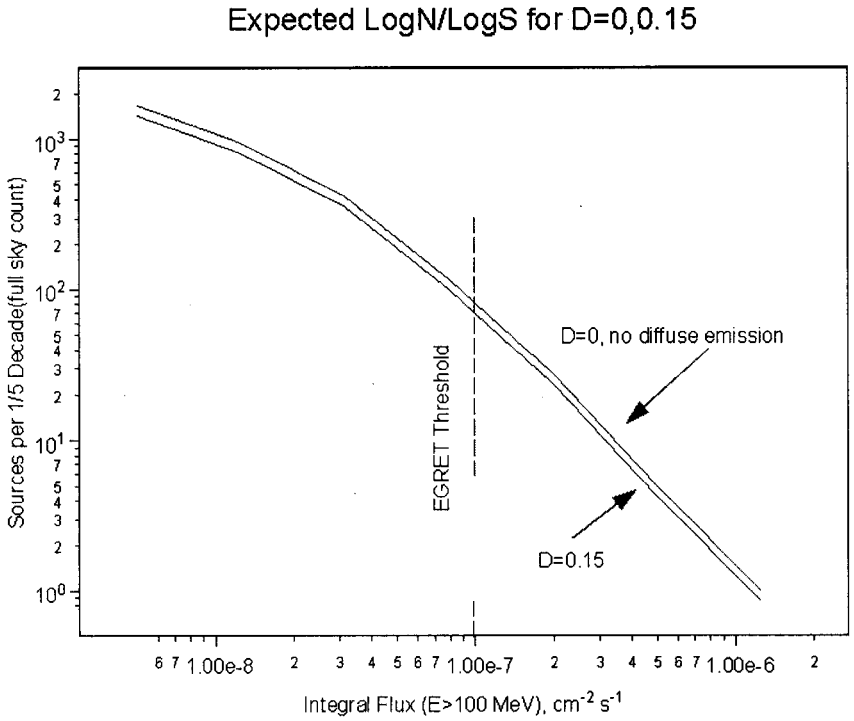

Figure 2.5: Expected logN/logS for various values of the Diffuse Ratio.

emission mechanism with a large time evolution were to be present, it would be necessary to alter our estimate of the D, given the form of our reconstructed logN/logS. This presents a model dependency which must be taken into consideration.

2.4 Existing LogN/logS Fit Models

There are many estimated luminosity functions in the gamma ray region, each of which suggests a different role for the emission from distant point sources. We first examine the observed background radiation, and then the current estimates given to the gamma-ray luminosity function.

2.4.1 Characteristics of the Observed EDGRB

The Extragalactic Diffuse Gamma-Ray Background (EDGRB), first detected by the SAS-2 experiment (Fichtel et.al, 1978), has been found to have an intensity given (Sreekumar et.al , 1998) by :

$$\frac{dN}{dE} = (7.32 \pm 0.34) \cdot 10^{-6} \left(\frac{E}{0.451 \text{ GeV}} \right)^{-2.10 \pm 0.03} (\text{cm}^{-2}\text{s}^{-1}\text{sr}^{-1}\text{GeV}^{-1}) \qquad (2.6)$$

SAS-2 showed a residual emission which was isotropic, and not associated with the galactic emission. Analysis of the EGRET data in the range above 100 MeV (Integrating 2.6) yielded a total emission of $((1.45 \pm 0.05) \cdot 10^{-5}$ photons cm^{-2} s^{-1} $sr^{-1})$, with a power law of about (2.10 ± 0.03) (Sreekumar et.al , 1998).

2.4.2 Estimates for the Gamma-ray Luminosity Function (GLF)

The "Luminosity Function" is the relation for the number of galaxies in a particular luminosity range. A luminosity function in the gamma-ray region has been approached in several ways: The observed luminosity distribution from EGRET was used (Chiang et.al, 1995) to extrapolate a luminosity function (in which sources were expected to behave as power-law emitters), and the better-characterized radio luminosity function (RLF) at 2.7 GHz was also used in a different attempt (Stecker & Salamon, 1996) to establish a linear relationship between the RLF and GLF in order to produce an estimated GLF around 100 MeV.

2.4.3 Direct Fitting of the GLF

The GLF was fit directly from EGRET data (Mukherjee, Chiang, 1999) and integrated to estimate that the entire contribution from unresolved blazers to the EGRB was $(3.0 \pm 1.0) \cdot 10^{-6}$ $(\mathrm{cm}^{-2}\mathrm{s}^{-1}\mathrm{sr}^{-1})$, only around a quarter of the entire estimated EGRB. However, this fit was also done without density evolution of the gamma-ray emissive AGN's, as the available EGRET data showed no significant evolution in comoving density of sources (that is, the density of sources estimated was static up to the EGRET sensitivity falloff, revealing only the portion of the logN/logS curve dominated by power-law behavior). Thus, it is possible that this result contains more systematic error than reported, however, it seems unlikely that this would invalidate the study, as an evolution in density of AGN would imply a lower contribution to the EGRB from unresolved objects than otherwise calculated.

2.4.4 Extrapolation of the GLF from the RLF

Among the motivations for this latter method was the assumption that high-energy emissive AGN sources are also visible in the radio region (Stecker & Salamon, 1996), a model supported by synchrotron self-compton (SSC) and external compton emission models. A linear relationship between the Radio Luminosity Function at 2.7 GHz and the GLF in the GeV region was assumed, with the linear factor being fit to match the GLF to the observed EGRET source catalog. The outcome of this work was consistent with an EGRB from background blazer emission of $(1.57) \cdot 10^{-5}$ $(\mathrm{cm}^{-2}\mathrm{s}^{-1}\mathrm{sr}^{-1})$. However, a constraint on this model was the requirement that the observed blaz-

ers from EGRET must account for the estimated GLF, given the sensitivity of the EGRET experiment. Thus, part of the actual GLF may be accounted for by a diffuse emission, rather than being wholly due to the sum of unresolved point sources. We are free (in principle) to impose new constraints on the GLF model, given that some of the net photon flux may be from a truly diffuse emission. However, it should be noted that the observed AGN population is plainly inconsistent with a large diffuse emission, as the GLF above the EGRET sensitivity is already similar to the emission from the observed AGN's, within standard errors. Above the EGRET PSS, the alteration in the number of observed sources at a given intensity due to a diffuse proportionate background of a few percent is statistically insignificant, however, the GLAST experiment should be able to differentiate between a GLF entirely accounted for by point sources and one partially comprised of diffuse extragalactic emission. In other words, if there is a diffuse background, then the depression in the LogN/LogS curve would become far more statistically obvious when the number of binned sources could be expected to change by more than a few in any given intensity bin (i.e. once GLAST data is available). Thus, both of these measurements are plainly inconsistent with a large diffuse emission, but either of them could well include a small emission within the confidence interval in which they are specified.

2.4.5 Evaluation of the Contribution of AGN, from a Reevaluation of the EGRB

As we have discussed, there are several primary ways to estimate the contribution of active galaxies to the EGRB, many of which rely upon an estimation of the luminosity function of the AGN (Stecker & Salamon, 1996). However, most of the estimates producing results implying a dominant contribution from AGN sources relied upon a correlation between gamma-ray and lower energy luminosity functions. This correlation is still debated(Mattox et.al, 1997). We expect the estimated luminosity function based on the AGN catalog from GLAST to merit an estimation of the AGN contribution without this assumption.

An unconstrained estimate was made for the contribution of AGN to the EGRB which considered only the data from EGRET (Chiang et.al, 1995). However, the AGN detected by the EGRET telescope on which the estimate was made were only present above about $10^{-7}\mathrm{cm}^{-2}\mathrm{s}^{-1}$ (as seen in Fig. 2.3), which led to large uncertainties.

Chapter 3

The GLAST Experiment

The GLAST (Gamma-Ray Large Area Space Telescope) mission is designed to be capable of being launched onboard a Delta-II Heavy Launch Vehicle. The spacecraft will contain all of the non-ground instrumentation for GLAST. The satellite instrumentation is composed of two experiments: the LAT (Large-Area Telescope), and the Gamma-ray Burst Monitor (GBM). All of their associated systems are covered in the following sections.

3.1 Motivation for GLAST

GLAST has a number of scientific objectives to accomplish, among which are: The resolution of AGN's, pulsars, and Supernova Remnants (SNR's), the modeling of the particle acceleration within these objects, understanding the spectral and temporal behavior of gamma-ray bursts and time-transient events, and to probe the high-energy emission region for energy spikes from proposed dark matter annihilations. (NASA, 1999) GLAST will provide data on an energy band previously not well explored (See Fig. 3.1). Furthermore, GLAST will be able to put a much lower bound on the level

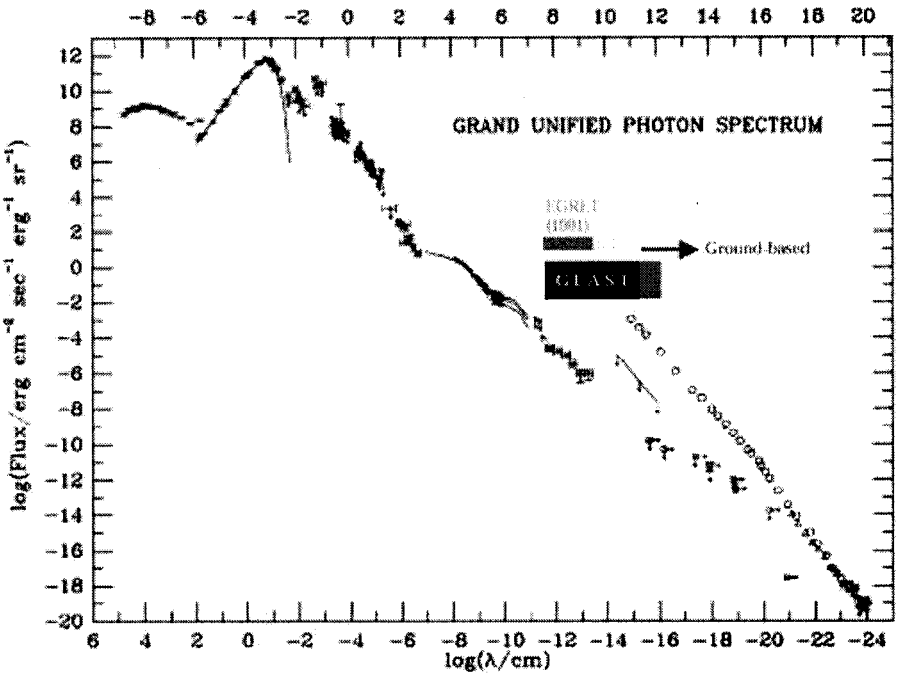

Figure 3.1: The Grand Unified Photon Spectrum, (Ressell & Turner, 1990), with EGRET, GLAST, and ground-based energy ranges.

of diffuse radiation in the gamma-ray band which is unresolvable, and corresponds to a diffuse emission mechanism in intergalactic space.

3.1.1 The EGRET Experiment

The Energetic Gamma-Ray Experiment Telescope (EGRET), was launched onboard the Compton Gamma Ray Observatory (CGRO). The predecessor experiment to GLAST, it searched for gamma rays in the range from 20Mev to around 30 GeV. EGRET used a spark chamber for direction estimation of incoming gamma-rays, and a calorimeter of NaI(Tl), much like GLAST. Tantalum foils for pair production were interleaved with tracking layers in the spark chamber, to allow EGRET the same ability for particle trajectory reconstruction as GLAST. A scintillating anti-

coincidence counter was also used. CGRO was launched in 1991, and underwent controlled reentry in 2000.

3.2 Mission Parameters

The GLAST spacecraft is expected to launch on a Delta-II rocket in 2007. It will be orbiting at an inclination of 28.5 degrees, in Low earth orbit (nominally about 550 km). Its required operating period is 5 years, and the goal will be for 10 years of data taking. The LAT has a field of view of more than 2.5 steradians, and sensitivity about 50 times that of its predecessor experiment, EGRET, at 100 MeV. At energies greater than 100 MeV, the current estimate for the threshold of source detection over two years of operation is around $4 \cdot 10^{-9} \mathrm{cm}^{-2} \mathrm{s}^{-1}$. Current estimates allowing for the instrument response function and time of mission suggest that the LAT will be able to locate sources to accuracies between 30 arc seconds and 5 arc minutes. A list of mission parameters can also be found at:

http://glast.gsfc.nasa.gov/science/overview/parameters.html.

3.3 Subsystems

The LAT is comprised of an array of tracker/calorimetry towers, all covered by the AntiCoincidence Detector and micrometeorite shield. Each tower contains a tracker module with conversion planes and silicon detectors, and a calorimetry module. A 4x4 array of these towers comprises the main body of the LAT. The subsystems are connected by a "Trigger and DataFlow System", which is responsible for analysis of

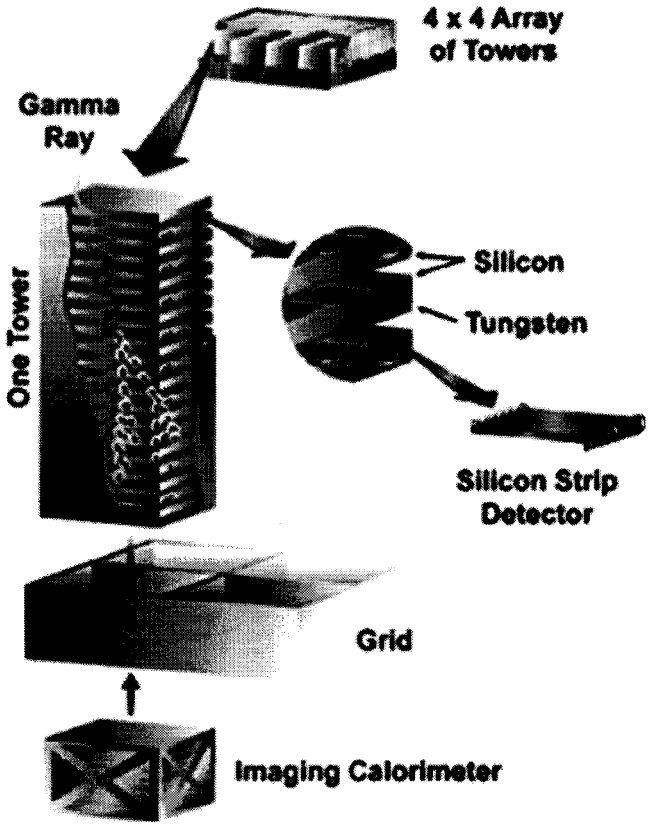

Figure 3.2: LAT Tracker/CAL subsystem detail

fast data, and rejection of data believed to be not representative of real gamma-ray events. This maximizes the throughput of useful data the instrument is capable of providing, and is considered a "subsystem" in and of itself. Figure AAA shows the detail of the LAT tracker and calorimetry models. Note the modular design of the LAT.

3.3.1 Spacecraft

The Spectrum Astro Corporation has been contracted to build the GLAST spacecraft. The spacecraft must contain the LAT, the gamma-ray burst monitor(Sec. 3.3.5), and

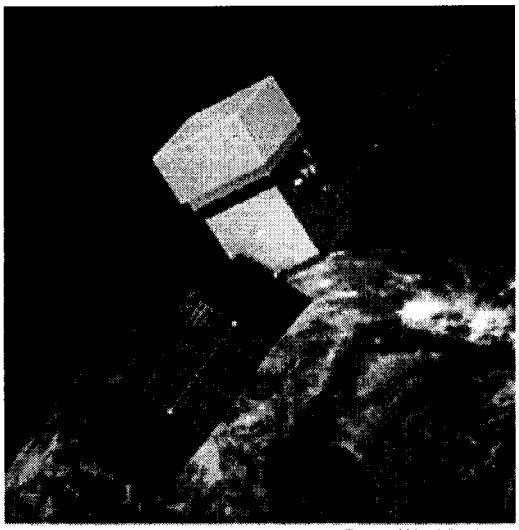

Figure 3.3: the Glast satellite in orbit (simulated)

two large solar panels, which will provide a power source. (See Fig. 3.3). A broadband connection will be utilized to allow GLAST to communicate data to several ground receivers. This is accomplished through the geosynchronous satellites in the Tracking and Data Relay Satellite System (TDRSS) network.

3.3.2 Tracker

It is the job of the tracker subsystem to convert cosmic gamma-rays into charged particles (via electron-positron pair conversion), and measure the paths of these particles, so that the data can be used to reconstruct the incident photon direction. The former goal is accomplished with a series of layers of 16 tungsten "conversion layers," which together provide about 0.5 radiation lengths of photon absorption (Gehrels, 1999), primarily through pair production. The first 12 of these layers are "thin," measuring 0.1 mm each, and the remaining 4 are "thick," measuring 0.72 mm each. Due to the

much larger statistical spread of reconstructed photon direction from the thicker or "back" planes of the detector, estimates in this work have been conducted considering only the thin conversion planes. In the energy ranges studied, a photon interaction with a dense nucleus is very likely to result in pair-conversion. After conversion, the subsequent tracking of charged particles is handled by a series of silicon strip detectors. These detectors consist of a thin sheet of bulk silicon (n-type), with strips of p-type doped silicon running in a single direction along the surface. A bias voltage is applied between the two types of silicon. As a charged particle passes through the strip detector, the electric field ionizes the silicon, freeing electrons and "holes" in the material. These holes then drift toward the p-type strips, and are collected, registering as "hits" to the detector strip. By interleaving layers of these detectors in different directions, then, the path of moving charged particles through the detector can be reconstructed into "tracks" corresponding to probable particle trajectory (see Fig. 3.4). Data from these "tracks" is sent to the "Trigger and DataFlow System", which handles the determination of a probable gamma-ray event.

3.3.3 Calorimeter

Thallium-doped Cesium-Iodide (CsI(Tl)) blocks are arranged in perpendicular hodoscopic (imaging) fashion in a matrix below the Anti-Coincidence Detector (ACD) and tracking planes. Silicon PIN Photodiodes are employed to react to the scintillation reaction as a charged particle passes through. 12 crystals of size 26.7 mm x 19.9 mm x 333 mm are individually optically isolated, and arranged in a layer, in which

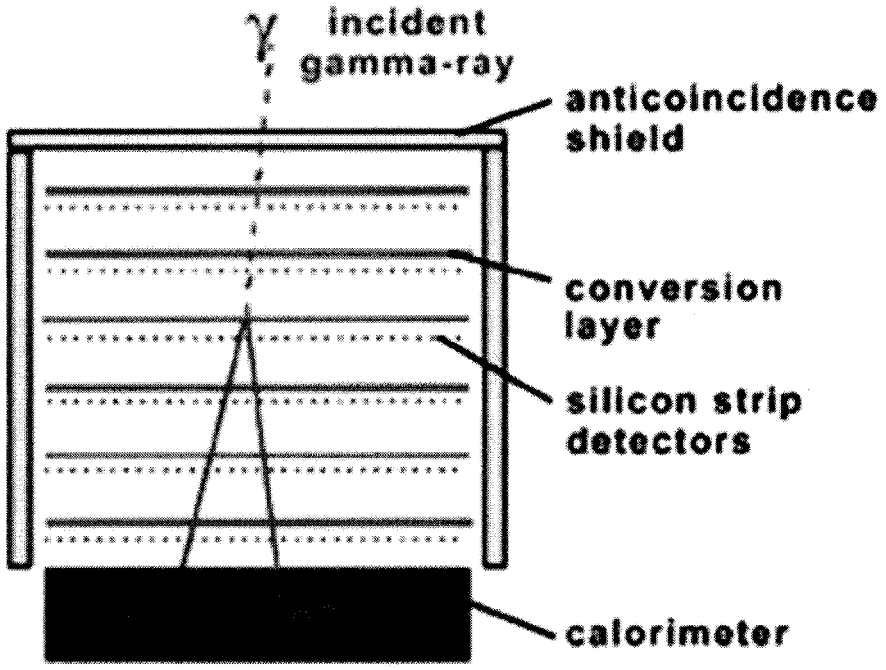

Figure 3.4: Gamma-ray pair conversion, detection, and calorimetry

each crystal faces the same direction. Eight such layers, each arranged in perpindicular fashion with respect to each other, constitute a calorimeter module, which resides "underneath" a module of the tracker system. (Johnson, 2001) The photodiodes on each end of each crystal allow for total calorimetry measurement, as well as giving some idea about the location of the incident particle causing the electromagnetic cascade within the crystal.

3.3.4 Anti-Coincidence Detector (ACD)

In order to reduce the number of false gamma counts due to cosmic rays entering the tracker planes, the ACD is designed to present minimal radiation length to gamma rays, while also recording incoming charged particles. This is accomplished by means

of a series of plastic scintillator tiles, each of which is "read out" through a series of wave-shifting fibers and photomultiplier tubes. In this way, incoming events likely to be due to cosmic ray interference can be ignored. Below about 3 GeV, there is a cutoff in charged particle flux thanks to the geomagnetic field, and above 30 GeV, the flux of cosmic rays falls faster than photons with energy, effectively helping the ratio of charged particles to incident photons. Though proton flux also vastly outnumbers photon flux at lower energy, both the interactions in the tracker as well as the calorimeter can be used to infer a proton event. Incident electrons, however, are more difficult to determine. Around 4 GeV, the electron flux is at or below 10 $m^{-2}\ sr^{-1}\ s^{-1}$. At the same energy, the diffuse gamma-ray flux is 0.003 $m^{-2}\ sr^{-1}\ s^{-1}$. To achieve the requirement expected of the ACD, then, (residual electron flux being less than 10% of the diffuse photon flux), The fraction of electrons improperly identified must be 0.00005 or less of the total electron flux (Ormes et.al, 2004). There is also a micrometeoroid shield, designed to protect the LAT from small objects incident upon it.

3.3.5 GRB Detection

In addition to the LAT itself, the Gamma-ray Burst Monitor (GBM) is the secondary instrument which will be onboard the GLAST spacecraft. The GBM is composed of a set of 12 low-energy scintillation detectors made of Sodium Iodide(NaI), and 2 High-energy scintillation detectors, made of Bismuth Germanate (BGO). The "low-energy" detection scale is from a few keV to around 1MeV, whereas the "high-energy" scale

is from around 0.15 keV to about 30 MeV. Together, these detectors will provide a method for detecting cosmic gamma-ray bursts, and allowing for spectral information on short-term gamma-ray events.

Chapter 4

Theory of source resolution

4.1 Observational Considerations

There are several issues that must be overcome to resolve faint sources amidst background, with low total photon counts. First, as the total number of photon events per source is very low, methods that would usually be performed on pixelated maps of photon counts (for instance, sequential source resolution and removal) will not work, as it is difficult to assign each photon to any given source. Furthermore, the GLAST positional accuracy for any given photon is highly dependent on energy, as well as being comparable to the expected angular separation between point sources. Because of this, any source resolution scheme will have to deal with the issue of source confusion. Also, the non-gaussian nature of the probability distribution function of reconstructed photon directions makes estimation of several source statistics (such as intensity and significance) difficult. Because of this, we will turn first to the theoretical considerations of point source resolution.

4.2 A Criterion for Source Resolution

We turn now to the interesting question of source resolution, in which we would like to know when we have resolved a source, given assumptions about the source density and distribution. As the null hypothesis in such a case is the absence of a source, the process of source resolution is really the calculation of the significance of the measurement of source counts. We consider a point source against a background. If the background flux is zero, measurements of the source location via the position of incoming particles are simply subject to small, random errors defined by the instrument response function (IRF), and therefore form a normal distribution about the source location, as discussed previously. It is important to note here that this assumes a gaussian instrument response, as the distribution of photons around the source direction will actually follow the IRF, so a non-gaussian IRF will produce a non-gaussian distribution. The non-gaussian case will be handled later in this work. However, as the incoming particles arrive randomly, the time distribution follows the Poisson statistics. Here, the probability of N particles arriving in a time T can be written

$$P_{r,T}(N) = exp\{-rT\}\frac{(rT)^N}{N!} \tag{4.1}$$

where r is the source rate. So the number of particles which will arrive in time T is simply

$$N = rT \pm \sqrt{rT} = \overline{N} + \sqrt{\overline{N}} \tag{4.2}$$

Now, we declare the "condition of resolution" to be the error in the measured rate being more than five times its own magnitude, or

$$N \geq 5\sigma_N, so N \geq 5\sqrt{N} \Rightarrow N \geq 25 \tag{4.3}$$

This standard result says that, if the background is unknown (but happens to be very small), we must observe 25 particles to be assured of having observed the source. However, for a nonzero background, what criteria establish the 5σ limit? We could say that, in a time T, that we will observe, on average, N_{OBS} total events, of which we estimate that $\overline{B}$ are from the background, and $\overline{N}$ from the source. It follows that our actual observed source counts will be:

$$\overline{N_{OBS}} = N_{OBS} + \sqrt{N_{OBS}} = \overline{B} + \overline{N} \pm \sqrt{\overline{B} + \overline{N}} \tag{4.4}$$

as each particle is randomly incident with respect to time, and thus the number incoming in a given interval follows the Poisson distribution (and variance). Thus, estimating the number of source counts:

$$\overline{N} = \overline{N}_{OBS} - \overline{B} \pm \sqrt{\overline{B} + \overline{N}} = \overline{N}_{OBS} - \overline{B} \pm \sqrt{\overline{N}_{OBS}} \tag{4.5}$$

and the variance of our measurement of the source counts $\overline{N}$ is just

$$\sigma_{\overline{N}}^2 = \sqrt{\overline{N}_{OBS}} \tag{4.6}$$

and, invoking the "resolution condition" of 5σ:

$$R_{Source} = R_{TOT} - R_{bgd} = r - R \pm \sqrt{\frac{\overline{n}}{T^2} + \frac{\overline{N}}{T^2}} = r - R \pm \frac{\sqrt{\overline{n} + \overline{N}}}{T} \tag{4.7}$$

Now, invoking the "resolution condition",

$$\frac{\overline{N}}{\sigma_{\overline{N}}} \geq 5 \Rightarrow \frac{\overline{N}}{\sqrt{\overline{B} + \overline{N}}} \geq 5 \tag{4.8}$$

Note that, when the background intensity is zero, 4.8 reduces to the familiar $\sqrt{\overline{N}_{OBS}} \geq 5$, implying that N_{OBS} (the number of total events) must be at least 25, as shown above. Also, as the source gets arbitrarily weak compared to the background ($B \rightarrow \infty$), 4.8 reduces to $0 \geq 5$, implying that the source cannot be resolved (again, as expected). Here, we run into an important issue of this kind of calculation - we must have a good way to estimate the relative strength of the background relative to the source. It might be valid to average the flux, say, 2σ from the source location, and consider that the "background flux", though that method may well be haphazard. We would like to understand more about resolution of a source in a background environment not necessarily "probable" - that is, not easily defined by a single flux. This is important, not only for the situation where we must resolve sources which are spatially close to one another, but also due to the fact that the background

emission may itself be larger than the galactic-emission model would presume, the extra flux being due to extragalactic diffuse processes. Further questions needing to be addressed include the resolving capability of the instrument in its actual environment. For instance, considering how many sources we are likely to see in several years' time, given their close juxtaposition and flux distribution. As will be shown later, this problem is perhaps best addressed by a numerical simulation of the data and instrument.

4.3 Error from Maximum Likelihood

We could also consider a source amid a background by using a maximum likelihood fit (as described in 4.10.1), and exploiting known results concerning the variance in such a fit. If we have a point source at a location (where θ denotes the distance away from the source), with a background flux r_b relative to the source flux density in the source direction (See sec. 4.7.1), and we can assume a known single-particle instrument variance σ^2, then it is reasonable to write the differential rate of incoming particles as:

$$\frac{dN}{d\Omega} = \frac{N}{2\pi\sigma^2_{IRF}}(exp\{-\frac{\theta^2}{2\sigma^2_{IRF}}\} + r_b) \tag{4.9}$$

where N is the number of signal data (counts from the source) arriving in a unit time. Now, for a small angle $d\theta$, we can say that $d\Omega = \pi d\theta^2$, and we make a change of variables, defining the variable u by

$$u = exp\{-\frac{\theta^2}{2\sigma_{IRF}^2}\} \tag{4.10}$$

Therefore,

$$\frac{dN}{d\Omega} = \frac{dN}{du}\frac{du}{d\Omega} = \frac{dN}{du}\frac{-u}{2\pi\sigma_{IRF}^2} = \frac{N}{2\pi\sigma_{IRF}^2}(u + r_b) \tag{4.11}$$

$$\frac{dN}{du} = \frac{-N}{u}(u + r_b) = -N(\beta + \frac{r_b}{u}) \tag{4.12}$$

where β stands for the relative source strength that we are measuring. For an unbinned maximum-likelihood fit, the inverse variance σ_β^{-2} is given by the relation

$$\sigma_\beta^{-2} = \frac{\partial^2(\log L)}{\partial\beta^2} = -\frac{\partial}{\partial\beta^2}\log(f(u,\beta)) \tag{4.13}$$

(Cowan, 1998) and $\int f(u)du = N$, the total number of measurements. Here, the function f is just

$$f(u) = \frac{dN}{du} = -N(\beta + \frac{r_b}{u}), \frac{\partial f}{\partial\beta} = -N \tag{4.14}$$

so

$$\frac{1}{\sigma_\beta^2} = \int (\frac{\partial f}{\partial\beta})^2 \frac{du}{f(u)} \tag{4.15}$$

and

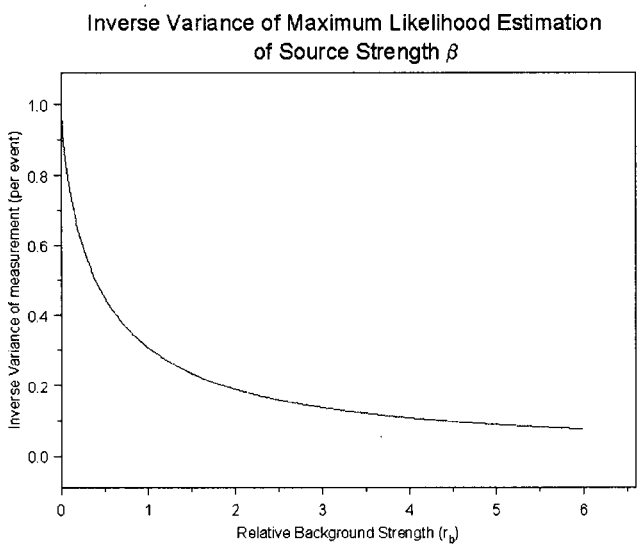

Figure 4.1: Inverse Measurement Variance from ML

$$\frac{1}{N\sigma_\beta^2} = \int_0^1 \frac{du}{(\beta + \frac{r_b}{u})} = -\int_0^1 \frac{u \cdot du}{\frac{u}{\beta} + r_b} = \int_0^1 \frac{u}{u + r_b} = [1 - r_b log(1 + \frac{1}{r_b})] \qquad (4.16)$$

(see Fig.4.1) The inverse variance shown is per event, and thus neglects the factor of N from eqn. 4.16. It is thus interesting to note that this result is simply the poisson counting result as the background becomes small, reproducing $\sigma_\beta = 1$ at zero background.

So, for a gaussian instrumental response function, we take the resolution condition to be the measured value of β to be more than 5 times its own uncertainty, which leads immediately to:

$$\beta^2 \geq \frac{25}{N}[1 - r_b log(1 + \frac{1}{r_b})]^{-1} \qquad (4.17)$$

as β is equal to 1, the condition of resolution can simply be reformed as:

$$N \geq 25[1 - r_b log(1 + \frac{1}{r_b})]^{-1} \tag{4.18}$$

4.3.1 The Estimated Point Source Sensitivity

More generally, we would like to employ the concepts in the preceding sections in order to give a general estimate of the total source flux at which the GLAST experiment could be expected to resolve any given point source after, say, 2 years of observation. Obviously, this calculation makes several assumptions, such as the necessary large angular separation of individual point sources, and a very small anisotropic component of the galactic diffuse radiation (which is a large problem at low galactic latitiude, thanks to the "washing out" of extragalactic point sources by the relatively high diffuse flux). The Point Source Sensitivity (PSS) calculated will be far more realistic at high latitudes by construction, and it is the high-latitude isotropic galactic intensity that we will use as the "background rate" for the calculation. Recalling section 3.4, we begin by constructing the probability distribution for incident particles to arrive at a certain angle, and with a certain energy:

$$G(E, \theta) = \frac{1}{2\pi\sigma^2_{IRF}(E)}(exp(\frac{-\theta^2}{2\pi\sigma^2_{IRF}(E)}) + r_b) \tag{4.19}$$

At this point, it is vital to note two differences between this and the calculation from section 4.3. Firstly, the uncertainty in the arrival direction of a single photon is a function of energy, E. This is the Point Spread Function (PSF) for the

detector at a particular energy. In principle, the PSF may also depend on incoming photon direction, certainly with respect to the detector's vertical axis, and possibly also azimuthally. Secondly, note that the factor r_b, which is the ratio between the background and source rate in the direction of the source, is also a function of E. This is not so surprising, considering that we have estimated a gaussian PSF as the instrument's response from a point source (Fig. 4.7), and that the FWHM of the gaussian peak depends on energy. Thus, for a particular total source rate ($cm^{-2}s^{-1}$) and background rate ($cm^{-2}s^{-1}sr^{-1}$) , the value of r will not be a constant in energy. Now, as particles are not equally likely to be incident with any energy, nor are they equally likely to be detectable at any energy, we must also include the energy spectrum of incoming particles, S(E), and the effective area, $A_{EFF}(E)$. Note that A_{EFF} also depends on the angle of incidence, thanks to both the geometry of the detector itself, and also specific details of its internal structure. For any relative direction with respect to the detector, the effective area will depend only on the energy. Thus, the angular dependence of effective area becomes an issue of satellite exposure, which will be discussed later. Thus, we have an explicit probability density given by:

$$F(E,\theta) \propto G(E,\theta)S(E)A_{EFF}(E) \tag{4.20}$$

For a given range of incident observed angles (from 0 out to an arbitrary angle, which, in principle, could approach infinity without substantially changing the calculation), and energies (for the sake of this calculation, 100 Mev to 100 GeV), we must

be sure to normalize the probability density to 1 over those regions. Here, we can now reform the function G as:

$$G(E,\theta) \propto \frac{1}{\sigma^2_{IRF}(E)}(\beta p(E,\theta) + b(E)) = \frac{p(E,\theta)}{\sigma^2_{IRF}(E)}(\beta + \frac{b(E)}{p(E,\theta)}) \tag{4.21}$$

Where β represents the quantity we are now trying to measure, p is the function representing the probability density of photons coming from any point source, and b is the probability density of photons from an isotropic background. We can then employ the earlier relation determining inverse variance of the estimation of β by a maximum-likelihood fit, as declared in eqn. 4.15. With this measure of the variance in measurement, we then use the resolution condition and source intensity to estimate the number of years necessary to observe the source in order to properly resolve it. The current estimated PSS for GLAST is around $3.0 \cdot 10^{-10}$ $(\mathrm{cm}^{-2}s^{-1})$, after 1 year. See Appendix B for a computational treatment of this problem and calculation of this figure. Given the assumptions made during the calculation, this can be seen as a lower limit to possible resolution over a given time period. Realistically, the PSS is better found through numerical estimation of simulated data, as will be done later in this work.

4.4 Wavelet Fitting Method

We will use the method of wavelet convolution in order to estimate point source locations and intensities from the map of photon events. The principle of this method

is that a function representing the image of a point source is convolved with the total image, yielding a new map corresponding to the value of this transform at every point, which (as we will see later) can be used to estimate the significance and total relative intensity of estimated sources in the map. We will use this estimation method to generate a preliminary "best guess" of source locations and fluxes, which will be input to the eventual maximum likelihood optimization algorithm. The method of wavelet transformations for angular point source resolution from incoming photons, over many scales and using different variations has been covered in many previous works (Terrier et.al, 2001; Damiani et.al, 1996, 1997; Starck,Murtaugh & Bijaoui, 1995). Most treatments consider photon maps examined in absence of any allowance for the differing instrument response of each incoming photon. Although the wavelet method involves the uncertainty of resolving the location of any given single event, allowances have not been made for the presence of many events at different uncertainties. Thus, past wavelet analyses were obtained from considering only a single angular size scale for any given photon source, and then "multiscale analysis" was performed by varying that intrinsic scale for source searches of different angular sizes (which for the purposes of high-energy astronomical source location, corresponds to different source energy indices for point sources of power-law energy distribution). As we will see, it is possible to use knowledge of the positional accuracy of each incoming photon in order to establish source intensity and significance for a single map of multichromatic photons (of varying energy), thus reducing processing time while

increasing confidence values for the source location. In the case of the EGRET mission analyses, the most commonly used method for source resolution was the method of maximum likelihood (Mattox et.al, 1996). However, the practical application of this method also included matching the locations of sources identified in other energy ranges to possible luminous objects in the gamma-ray region. In this way, our confidence of finding actual sources was increased. As the GLAST instrument is estimated to resolve around 1400 sources in the period of a year, by our estimation methods(see Sec. 6.1), such "source identification" will not be possible for all of them, and thus a method involving only incident photon information is necessary to determine a catalog of likely source locations.

4.4.1 The Continuous Wavelet Transformation

The Continuous Wavelet Transformation (CWT) is defined as follows:

$$W_I(\mathbf{b}, \alpha) = \int d^2\mathbf{r}\psi(\frac{\mathbf{r}-\mathbf{b}}{\alpha})I(\mathbf{r}) \tag{4.22}$$

where I represents the image data, and ψ is a function loosely modeling our point-source, also called the Analyzing Wavelet Function (AWF). Here, $\mathbf{r}$ and $\mathbf{b}$ represent unit vectors on the sphere, and α is the "dilation factor", or scale of the AWF. In the more general case of wavelet transformations for signal processing or image compression, the AWF must be considered to vary with position $\mathbf{b}$ and dilation factor α. However, in our case, we are considering only the convolution value of the AWF centered upon a given location where we are "testing" for the presence of a point

source.

4.4.2 The Analyzing Wavelet

We first turn to the problem of devising an appropriate function to use as a "model" for our source image. The AWF has a few important features to consider, such as applicability for representing the new data, as well as a necessary insensitivity to artifacts of the detector and unusable aspects of the image, such as constant background noise and/or linear gradients. We can establish the criteria for a usable AWF as follows:

- The AWF must integrate to zero, thereby ensuring insensitivity to uniform background noise,
- The AWF should furthermore be insensitive to linear gradients of photon density across the map,
- The AWF should be of a form which closely represents the distribution of incoming photon detections.

The AWF thus employed most often for these purposes is the so-called "Mexican Hat Function," of the form:

$$\psi(\frac{\mathbf{r}-\mathbf{b}}{\alpha}) = (2 - |\frac{\mathbf{r}-\mathbf{b}}{\alpha}|^2)exp(\frac{-1}{2}|\frac{\mathbf{r}-\mathbf{b}}{\alpha}|^2) \tag{4.23}$$

or

$$\psi(u) = 2(1-u)e^{-u} \tag{4.24}$$

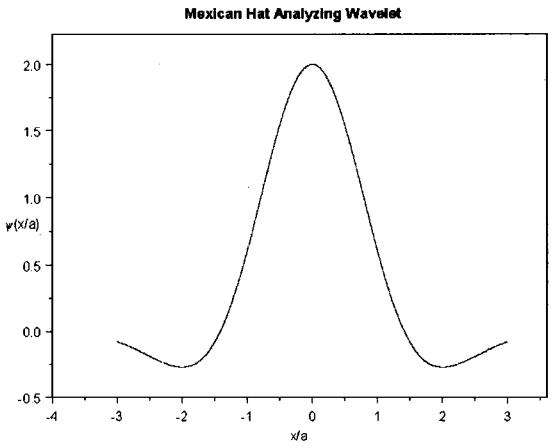

Figure 4.2: the Mexican Hat Analyzing Wavelet Function

where

$$u = (\frac{1}{2})(\frac{\mathbf{r}-\mathbf{b}}{\alpha})^2 \tag{4.25}$$

Note here that, as the AWF is symmetric, ψ can only depend radially on $\mathbf{r}$ and $\mathbf{b}$ as $\frac{\mathbf{r}-\mathbf{b}}{\alpha}$. In this way, we reconsider the AWF as a function of just position $\mathbf{r}$ and dilation factor α , considering $\mathbf{b}$=0. [See Fig. 4.2]

4.4.3 Choice of Wavelet Dilation Factor

Given knowledge of the position uncertainty of events as a function of their energy, we turn to the problem of choosing the dilation factor α(E). In order to estimate the optimal factor, we first consider a (monochromatic) gaussian source of effective size σ_s:

$$I(\theta) = \frac{\exp(\frac{-\theta^2}{2\sigma_s^2})}{2\pi\sigma_s^2} \tag{4.26}$$

As there is no background, I(r) is the Point Spread Function (PSF) of this source. We will attempt to optimize the resolution power of the CWT, given this PSF. Doing the integral to find the Continuous Wavelet Transformation (Damiani et.al, 1997),

$$W_I(\theta, \alpha) = \frac{1}{1 + (\sigma_s^2/\alpha^2)^2}(2 - \frac{\theta^2}{\alpha^2 + \sigma_s^2}) \exp(\frac{-\theta^2/2}{\alpha^2 + \sigma_s^2}) \tag{4.27}$$

It has been shown (Damiani et.al, 1997) that the peak of this function is maximal (and therefore a greatest sensitivity to point sources is found) at:

$$\alpha_{max} = \sqrt{3}\sigma_s \tag{4.28}$$

In our case, we expand this definition to apply to photons of any energy E, and corresponding angular scale σ(E), and define:

$$\alpha(E) \equiv \sqrt{a}\sigma(E) = \sqrt{3}\sigma(E) \tag{4.29}$$

where $a = 3$ for gaussian sources. Thus, a is defined as the relative scale factor, or "dilation coefficient" for the Wavelet Transformation. It should be noted that this calculation must be reconsidered for the case of nongaussian sources, as in the case of real instrument data.

4.4.4 Multichromatic Extension of the Method

Data from the GLAST mission, due to low total photon counts and the corresponding binning difficulties, is best treated as a set of individual events in the vicinity of some angular direction than as a map of noisy intensity, as might be done in X-Ray data analysis. Furthermore, the point-spread of incoming photons has a strong dependence on energy, necessitating either an estimation of the "effective" PSF of a source of given spectrum beforehand (Damiani et.al, 1996, 1997), or a careful treatment of the CWT to include the PSF of each photon in the set, as we will attempt here. With the above identifications for the CWT and AWF, the transform can be rewritten, now as a function only of the scale factor:

$$W(a) = \int d^2\mathbf{r}\psi(\mathbf{r}, a(E))I(\mathbf{r}, E) \tag{4.30}$$

where we use a(E) to represent the scale coefficient for each photon. However, we have the further requirement that the scale factor a is dependent upon the energy of each photon, so we rewrite the image function I as the sum of many individual photon events, each with a location and corresponding dilation coefficient a. In this way, we are acknowledging that the image function actually has three dimensions, two angular ones and energy.

$$I(\mathbf{r}, E) = \sum_i \delta(\mathbf{r} - \mathbf{r}_i)\delta(E - E_i) \tag{4.31}$$

Thus, we have preserved the dependence of the image function on the energy of each

photon. Then we rewrite the CWT:

$$W(\mathbf{r},a) = \int d^2\mathbf{r} \sum_i (\delta(\mathbf{r}-\mathbf{r}_i)\delta(E-E_i)\psi(\mathbf{r},a(E))) = \sum_i \psi(\mathbf{r}_i, a(E_i)) \tag{4.32}$$

The equivalence of this treatment can be seen from the limit of an infinitesimally small energy binning structure in the computation of the transform. Consider a multichromatic source as the superposition of every photon event, each with a distinct energy:

$$I(\mathbf{r}) = \sum_i I_{E_i}(\mathbf{r}) \tag{4.33}$$

The multichromatic transformation will thus give the same result as the monochromatic CWT done on each photon individually:

$$W(\mathbf{b}) = \sum_i \psi(\mathbf{b}, a_i) \tag{4.34}$$

In this way, the CWT is performed on a map of multichromatic photons in an unbinned way. This is important to note, since the Wavelet Transformation is often applied to data by spatially binning the data and then using the Discrete Wavelet Transformation (DWT) over it. In the multichromatic treatment, computing the CWT is possible without the need for binning considerations, either in angular direction or energy (See Appdx. B).

4.4.5 Variance in Flux Estimation

Considering an incoming particle distribution as a gaussian against a constant background:

$$I(\mathbf{r}) = B + \frac{N\exp(-r\theta^2(\mathbf{r})/2\sigma^2)}{2\pi\sigma^2} \tag{4.35}$$

The value of the wavelet transformation is thus proportional to the source counts, even in the presence of a uniform (or linearly varying) background:

$$W_{Peak}(a) = N_{src} = C\int d^2\mathbf{r}\psi(\mathbf{r}/a)I(\mathbf{r}) \tag{4.36}$$

where C is the normalization coefficient needed to make W an unbiased estimator of the source counts:

$$C(a) = [\int d^2\mathbf{r}\psi(\mathbf{r}/a)I(\mathbf{r})]^{-1} \tag{4.37}$$

Given Equation 4.37, it is straightforward to prove that W_{Peak} is an unbiased estimator for N. Considering a sample of k photons at locations $\mathbf{r}_i$, the expectation value for the peak value of the CWT is:

$$E(W_P) = \int\cdots\int W_P(\mathbf{r}_1\cdots\mathbf{r}_k)f(\mathbf{r}_1)\cdots f(\mathbf{r}_k)d\mathbf{r}_1\cdots d\mathbf{r}_k \tag{4.38}$$

where $f(\mathbf{r}_i)$ is the probability density for photon i being found at location $\mathbf{r}_i$, given a source of counts N, and $W_P(\mathbf{r}_1\cdots\mathbf{r}_k)$ is the value of the Wavelet Transformation,

given the incoming photons 1 through k. Thus, we note that $f(\mathbf{r}_i) = I(\mathbf{r}_i)$, and so, using eqn. 4.31, we find

$$E(W_P) = \sum_i d^2 r C\psi(r) I(r) = \sum_i C\psi(r_i, a_i) = N \tag{4.39}$$

Likewise, we can estimate the variance of the measurement of N, by considering the expectation value for N^2:

$$Var(W_P^2) = \sum_{i,j} \int \int N(\mathbf{r}_i) N(\mathbf{r}_j) f(\mathbf{r}_i) f(\mathbf{r}_j) d\mathbf{r}_i d\mathbf{r}_j \tag{4.40}$$

$$= \sum_{i \neq j} \int d^2\mathbf{r}_i \psi(\mathbf{r}_i) I(\mathbf{r}_i) \int d^2\mathbf{r}_j \psi(\mathbf{r}_j) I(\mathbf{r}_j) + \sum_{i=j} \int d^2\mathbf{r}_i \psi^2(\mathbf{r}_i) I(\mathbf{r}_i) \tag{4.41}$$

$$E(N\frac{W_P^2}{N}) = E(\sum_{i \neq j} N\psi(\mathbf{r}_j) + \sum_i \psi^2(\mathbf{r}_i) I(\mathbf{r}_i)) + V(N) \tag{4.42}$$

$$= N(N-1) + \int d^2\mathbf{r}_i \psi^2(\mathbf{r}_i) I(\mathbf{r}_i) + N \tag{4.43}$$

where we have allowed for poisson fluctuations in the estimation of N. Then we remember the form of the variance of N:

$$V(N) = E(N^2) - [E(N)]^2 \tag{4.44}$$

So equations 4.39 and 4.40 lead immediately to the variance of the measurement of the source counts N:

$$\sigma_N^2 = \int d^2r |\psi(\mathbf{r}/a)|^2 I(\mathbf{r}) \tag{4.45}$$

With the identification $a = \sqrt{3}$, and defining the ratio of background to source intensity in the source direction, $b \equiv B(\frac{N}{2\pi\sigma^2})^{-1}$, we can calculate the variance in the measurement of N, for gaussian sources (See Appdx. H):

$$\sigma_N^2 = N(1.289 + 2.370\ r_b) \tag{4.46}$$

Thus, the significance of finding a source can be calculated.

4.4.6 Motivation

There are certainly regimes of source behavior in which the multichromatic transformation should outperform the traditional CWT. For a multichromatic point source with a power law distribution: $P(E)dE = kE^{-\eta}$ The continuous photon distribution for a source at the origin will be:

$$I(\mathbf{r}) = \int dE\ P(E)\ \frac{1}{2\pi\sigma^2(E)} exp(\frac{-|\mathbf{r}|^2}{2\sigma^2(E)}) \tag{4.47}$$

The CWT can then be computed using either a single σ, or using our multichromatic treatment. The result can be seen graphically with a numerical computation of the standard and multichromatic Wavelet transformation of a source. In this case, we choose a point source located at the spatial position l=b=0, with a power-law index of 2 (Fig.4.3).

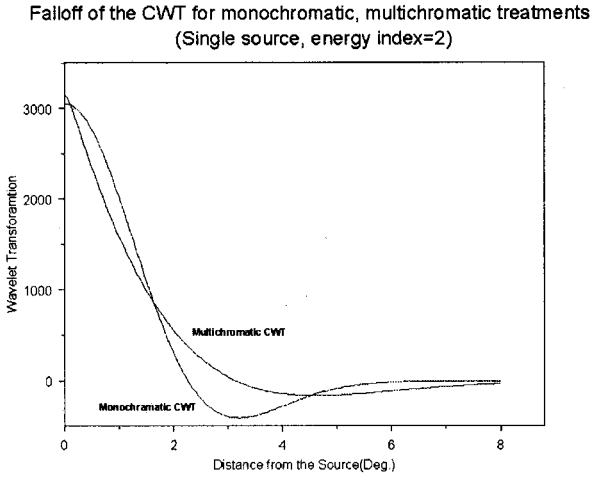

Figure 4.3: CWT Falloff for standard, multichromatic analysis

The prominence seen in the multi-chromatic peak is aided by a hardening of its localization, as compared to the mono-energetic analysis. For this reason, the source should be more precisely resolved by the multichromatic analysis. A few features are immediately obvious in this new transform, most notably that the negative annulus around the peak of the transform has now been "spread out" over a much larger area. This is due to the fact that each photon event now corresponds to a point on the AWF determined by both its position and energy. In the monochromatic treatment, then, all photons at a particular distance away from the point source would correspond to a point on the AWF of the same value (thus, all photon events within the negative region contribute to the negative value of the transform there, but this is not so in the multichromatic transform. Secondly, the value of the peak of the multichromatic CWT is somewhat higher than that of the transform made with a single dilation factor. This can be thought of as an enhanced resolution capability in the same

way that the ratio of the peak transform to the dilation factor was maximized 4.4.3. However, as we intend to use the value of the CWT to estimate the total rate of photons incoming from a given source, we must be careful to develop the case for the estimated intensity of a source given the CWT with the multichromatic treatment.

4.5 Single-Source Resolution Results

We turn now to the results of the wavelet method in determining source intensity, location, background intensity, and the significance of source resolution.

4.5.1 Estimate of Source Counts and Intensity

The wavelet transformation has been shown to provide an estimate for the number of photon counts coming from a potential source (Damiani et.al, 1997). Considering a gaussian PSF, an estimate for the contribution of an incoming photon to intensity of a given source can be made. With the definition of C from eqn.[4.37], eqn.[4.39] leads to an estimation for the source counts N, from a source at $\mathbf{b}$:

$$N(\mathbf{b}) = CW(\mathbf{b}), C = \frac{8}{9} \tag{4.48}$$

The multichromatic variant on this method also yields the same result, as can be seen from considering a multi-chromatic source as the summation over several subsources binned in energy, as done in section 4.4.4. Considering every photon in the map, it is trivial to consider the wavelet transform maximum by rewriting the contribution to W of each binned photon:

$$N(\mathbf{b}) = C \sum_i \psi(\mathbf{r}_i - \mathbf{b}/\sqrt{a_i}) \tag{4.49}$$

Thus, the estimate of the intensity of a multichromatic source is just the scaled wavelet transformation value at that location. Note that the factor of C will change for nongaussian sources, as is explored below for the case of the GLAST instrument response.

4.5.2 CWT as an Estimator of Source Intensity

The value of the peak of the wavelet transform is an unbiased estimator for the intensity of a point source by the preceding arguments. We are now equipped to produce several simulations of a source, and, in each case using our estimation of its intensity as a measure, follow the source intensity measurement and variance thereof as we observe more and more source counts (See Figs.4.4,4.5). We expect the number of reconstructed source counts to be distributed normally about the actual number of incoming photons. The expected deviation should increase as $(N_{src})^{1/2}$.

The estimated source flux is asymptotically equal to the actual value as the number of observed source counts becomes large. This is the expected result of the simulation method when the background intensity is negligible. We will return to this calculation, with varying background intensity, in the following sections.

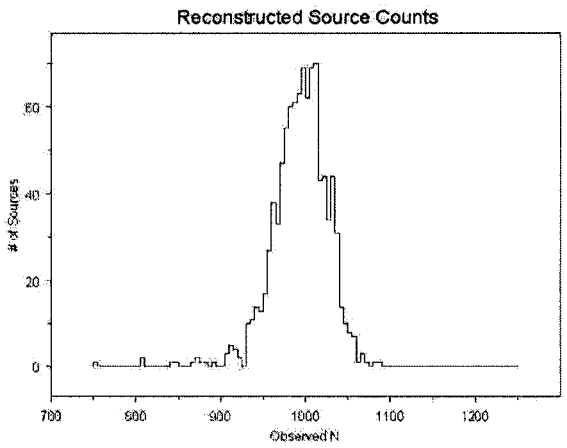

Figure 4.4: Reconstruction: For a sample of n=1000 observations of a source, each of events N=1000, we reconstruct the following distribution of N_{Obs}

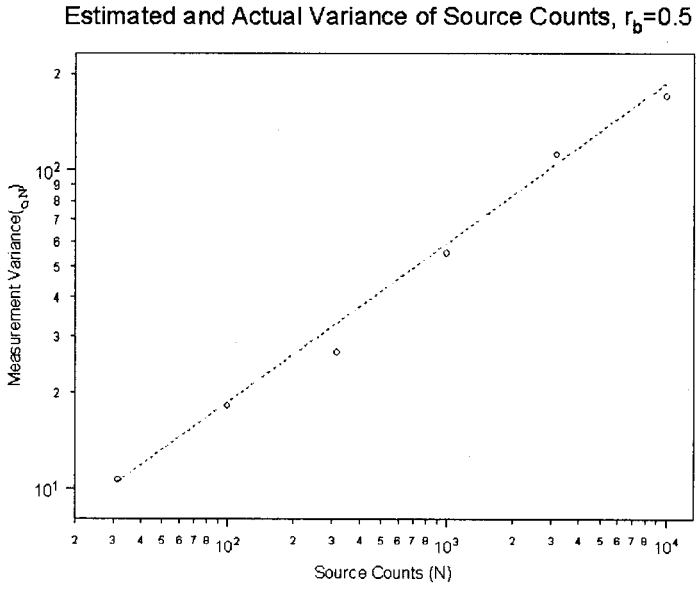

Figure 4.5: Source counts vs. standard deviation of the reconstruction of source counts, for sources with a background of r_b=0.5. Dotted line is theory, while points are calculated values from simulated data.

4.5.3 Background Estimation (Gaussian Smoothing Filter)

The background is estimated by using a gaussian smoothing filter to find how many photons come from a given direction, on average. The smoothed map is produced by convolving a gaussian over the data, and this gaussian must be defined with some normalization and width. For this purpose, we use the parameters corresponding to the incoming source photons to be smoothed. First, we consider a single incoming photon with detected direction $\mathbf{r}$, and note that the normalized probability density that the photon represented by index i actually came from location $\mathbf{b}$ is given by:

$$P_i(\mathbf{b}) = \frac{1}{2\pi\sigma_i^2} \exp\left(\frac{-(\mathbf{r_i} - \mathbf{b})^2}{2\sigma_i^2}\right) \tag{4.50}$$

Thus, for the entire catalog of photon detections, the sum over each of these probability densities is:

$$P(\mathbf{b}) = \sum_i P_i(\mathbf{b}) \tag{4.51}$$

This is therefore the probability density for the total number of photons per unit solid angle, in a given direction. This, it is an estimator for the sum of the background and source counts in that direction. Since the wavelet transformation gives us an estimate for the counts just from the source, the intensity from a possible source in the direction $\mathbf{b}$ (of point spread σ) is subtracted to establish an estimate for the background:

$$B(\mathbf{b}) = P(\mathbf{b}) - \sum_i \frac{W_i(\mathbf{b})}{2\pi\sigma_i^2} \tag{4.52}$$

4.5.4 Significance Calculation

With knowledge of the source counts and background, a calculation of the significance for source detection can be made by calculating the variance in the estimation of the source flux. Considering the wavelet dilation factor for a given photon, α_i, and the angular distance from the source location of that photon, θ_i, we make the definition of u for photon i:

$$u_i = \frac{\theta_i^2}{2\alpha_i^2} \tag{4.53}$$

The AWF then becomes:

$$\psi(u) = C(1-u)exp(-u) \tag{4.54}$$

where C is the coefficient given to the CWT to make it an unbiased estimator of source counts (See Eqn. 4.37). The variance of the measurement of N is:

$$\sigma_N^2 = [\int_0^\infty duS(u)]^2 \int_0^\infty \psi^2(u)(S(u) + r_b S(0)) \tag{4.55}$$

where S(u) is the PSF of a photon observation (Eqn. 4.45),and the remaining integral over S is simply the normalization factor of N. The variance of the unbinned maximum likelihood method is:

$$\sigma_N^2 = \frac{1}{\int_0^\infty S(u)du} \int_0^\infty \frac{S(u)^2}{S(u) + r_b S(0)} du \tag{4.56}$$

where u is as defined in eqn. 4.10 in this latter equation. The inverse variance of the wavelet method is then used with an estimation of the background to make a significance estimate for a source at any given location. For a gaussian S, the ratio of inverse variances between the ML and the CWT methods is calculable: (see Appdx. G).

4.5.5 Maximization of the CWT

As the significance is calculated (and cut against a threshold) at local maxima of the wavelet transformation, it is necessary to have a quick and robust maximization method at hand for locating these maxima. We first determine the gradient of the wavelet transformation, and then use the method of gradient ascent to locate the nearest maximum. From the sum definition of the multichromatic CWT:

$$W_I = \sum_i \psi(u_i) \tag{4.57}$$

We can then estimate the gradient of the CWT by exploiting the radial symmetry of the AWF. Thus,

$$\nabla W(\mathbf{b} = 0) = \frac{\partial W}{\partial r}\hat{r} = \sum_i \frac{\partial}{\partial r}[\psi(u_i)]\hat{r}_i \tag{4.58}$$

where $\hat{r}_i$ is the unit vector from the origin (b=0) to photon event i. Now,

$$\frac{\partial\psi(r)}{\partial r} = \frac{\partial\psi}{\partial u}\frac{\partial u}{\partial r} = \frac{cr}{a\sigma^2}(u-2)exp(-u) \tag{4.59}$$

where we have rewritten the factor of α in terms of a (as in equation 4.29) for ease of use with our numerical algorithm. Thus, the photons can be analyzed to find the spatial gradient vector of the CWT at any point. In this way, the gradient of the wavelet transformation can be found in the same summed fashion as the transformation itself. Likewise, we calculate the second spatial derivative:

$$\frac{\partial^2\psi(r)}{\partial r^2} = \frac{cr^2}{a^2\sigma^4}(3-u)exp(-u) + \frac{\partial\psi(r)}{\partial r}/r \tag{4.60}$$

Then, we employ the method of gradient ascent to locate the maxima of the transformation, beginning with the locations of local maxima of incoming photons (the spatial bins with the most photons). Following Newton's method, the estimated location of the CWT maximum is altered iteratively:

$$r_{i+1} = r_i - k\frac{\psi'(r_i)}{\psi''(r_i)} \tag{4.61}$$

where k is a small positive constant, equal to 1 in the standard "Newton's Method" usage. In our implementation, k is variable in case of source confusion or other difficulty. This is a relatively useful way to approach maximization, and carries several bonuses. In addition to being a relatively fast way to approach the wavelet peaks, it also allows us to move in arbitrarily small increments in order to do so, thus outperforming the alternate method of binning the CWT and noting the local

maxima.

4.5.6 Error Circle Calculation

For a source with an isotropic background, we consider the estimator for the position of the source. Every incoming photon will be weighted by both the position uncertainty and the value of the wavelet transformation, and we must consider many photons from the background as well as the source. So, considering that a source is located at the local maximum of the CWT:

$$\nabla_{\mathbf{b}} \sum_i \psi(\frac{\mathbf{r}_i - \mathbf{b}}{i}) = 0 \tag{4.62}$$

We consider the Taylor's series approximation centered on $\overline{\mathbf{b}}$, the estimated location for the source:

$$0 = \sum_i \psi'(\frac{\mathbf{r}_i - \overline{\mathbf{b}}}{a_i}) + \frac{(\mathbf{r}_i - \overline{\mathbf{b}})}{a_i} \psi''(\frac{\mathbf{r}_i - \overline{\mathbf{b}}}{a_i}) \tag{4.63}$$

$$\sum_i \frac{x_i}{\sigma_i} \psi''(\frac{\mathbf{x}_i - \overline{\mathbf{b}}}{a_i}) = \sum_i \frac{\overline{\mathbf{b}}}{\sigma_i} \psi''(\frac{\mathbf{x}_i - \overline{\mathbf{b}}}{a_i}) \tag{4.64}$$

This approximation is therefore good for photons close to the maximum of the CWT. The estimator for the location of the source is just:

$$\overline{\mathbf{b}} = \frac{\sum_i \frac{\mathbf{x}_i}{\sigma_i} \psi''(\mathbf{x}_i/a_i)}{\sum_i \frac{1}{\sigma_i} \psi''(\mathbf{x}_i/a_i)} \tag{4.65}$$

a weighted average of the photon position, with a weight of $\frac{\psi''(\mathbf{x}_i/a_i)}{\sigma_i}$. Likewise, the variance of this measurement can be written as just the variance of the weighted

mean:

$$V(\bar{b}) = E(\bar{b}^2) - [E(\bar{b})]^2 = \frac{\sum_i \psi''^2(\mathbf{x}_i/a_i)}{(\sum_i \frac{1}{\sigma_i}\psi''(\mathbf{x}_i/a_i))^2} \tag{4.66}$$

4.5.7 Extended Sources

An important caveat of the above method is that the background behind a point source does not vary faster than the scale defined by the AWF. However, in the multiscale treatment, some events may have an effective AWF scale much larger than the background fluctuation. A particularly important example is the diffuse emission from the galactic plane at all energy scales in the data used by the GLAST experiment. If the background varies quickly on the size scale of the AWF (quadratically or with higher order), then the "background cancellation" due to the negative tails of the AWF will no longer give a proper result. In the case of the galactic plane, the photons with instrument response uncertainty of around the size of the galactic plane itself (about 10 degrees galactic latitude) give a spurious positive result to the CWT, in the region of the plane. In order to deal with this problem, a possible solution has been implemented: The "running cutoff" approach, where only events of a suitable size scale are used at any given point in the spatial analysis (for GLAST, this means an energy cutoff of around 1 GeV on the galactic plane). It is also possible to use a "background foreknowledge" approach, wherein the CWT of the expected background is made, and then subtracted from the analysis made from all photons. In practical application, determination of source statistics is often done by considering only high-

latitude regions in the necessary analyses (such as disallowing results within 15 degrees of the galactic plane).

4.6 Application to Simulated GLAST Data

4.6.1 Multichromatic source efficiency across intensity

A necessary calculation to be made is the efficiency of the detector and the numerical resolution method. We produce a sample of simulated source, and reconstruct sources from their data, using a parameterization of the instrument response (Sec. 4.6.2) to estimate data uncertainty (Fig. 4.6). The efficiency plotted represents the ratio of the sources detected in an intensity bin to the actual number of sources there. In the region of high efficiency, this number may fluctuate above 1, as sources from one bin may be detected in another. The tolerances shown for resolution are 1 degree of angular separation on the sky, and $\pm 20\%$ of the total source intensity.

Using this method on simulated data from the GLAST experiment gives results in keeping with the expected point source sensitivity of the apparatus. We estimate the Point Source Sensitivity (PSS), the intensity that a source must reach to be detected in a given time scale (See Appdx. A). For sources with a characteristic power law index of 2.2, as found in earlier analyses of AGN objects (Lin et.al, 1999), the efficiency of detecting sources with this method closely matches the expected PSS of point source resolution by GLAST. For the period of a month, for instance, the intensity of a source necessary to make it likely that the MCWT will resolve it is roughly equal to the PSS for an isolated source for the same time period (See Appdx.

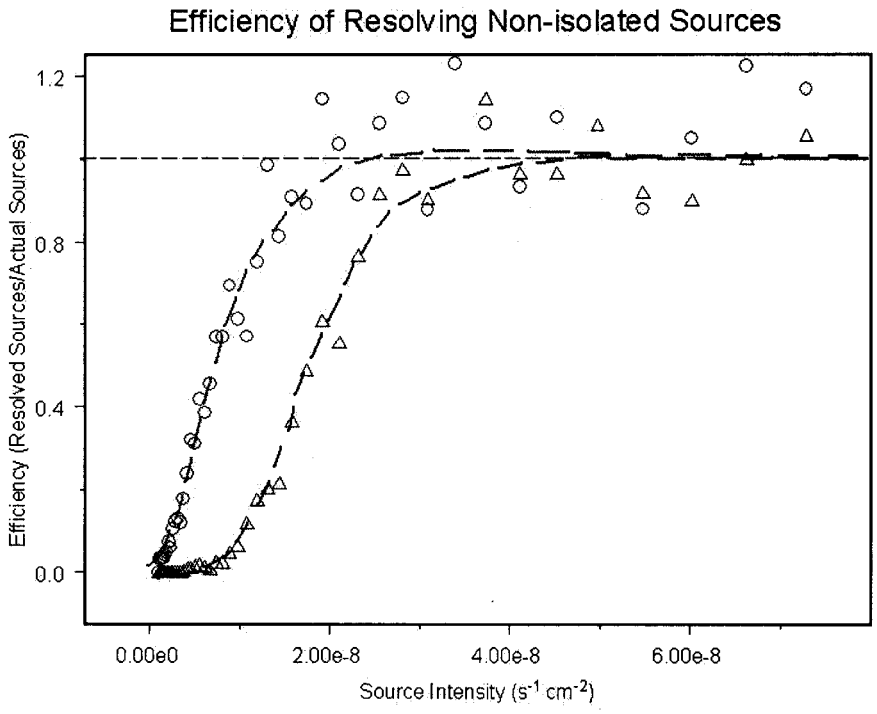

Figure 4.6: efficiency graph for b=0, 1 week/month. Lines are drawn.

A). As the MCWT method is here employed to find sources in a dense source catalog, it cannot be quite as efficient at doing so as the Maximum-Likelihood fit, which is calculated considering an isolated source in a region of high galactic latitude.

4.6.2 GLAST PSF and Source Counts Estimation

The GLAST PSF has been parameterized thus:

$$S(u,s) = \frac{1}{1+u+s\frac{u^2}{2}} \tag{4.67}$$

(Burnett, 2004), where s is a "shape parameter" that varies between 0 and 1 for most conditions, and u is the scaled radial component , $u = \frac{\theta^2}{2\sigma^2}$. Given this, and the

generalized Analyzing Wavelet Function (Eqn. 4.54),we can consider the normalized wavelet transformation:

$$W_I(s) = C \int du\psi(u)S(u,s) \tag{4.68}$$

here, again, C is the constant necessary to make the WT an estimator of the source counts, N.

$$C = \frac{\int_0^\infty duS(u,s)}{\int_0^\infty du\psi(u)S(u,s)} \tag{4.69}$$

In practice, each photon must be transformed individually, and so the normalization is used as a weight to the contribution of each photon.

4.6.3 Significance

Given a source with a background flux B, and PSF S:

$$I(b,u,s) = S(u,s) + B \tag{4.70}$$

we can then calculate the variance of the measurement of N:

$$\sigma_N^2 = C^2 \int_0^\infty du\psi^2(u)[S(u,s) + r_b\ S(0,s)] \tag{4.71}$$

and thereby the significance of measurement of a source with N counts.

4.7 Estimated Point Source Significance

Suppose we have a source made of a set of energy bands $E_1 \cdots E_k$, each with corresponding effective point spread I, total number of detected signal events N_I, and ratio of total background flux to signal flux from that energy in the source direction r_I. We wish to estimate the relative signal strength of each band, and then add them together (taking variances of each into account) in order to estimate the total signal strength. As shown in Appendix F, we found that $\sigma_{a_i}^2 = N_i[1.28 + 2.37r_b]$, for energy band E_i. This is true for a monochromatic source of total counts N. Thus, measuring the signal strength of the combined source, we have $S = \sum_i S_i$

4.7.1 Numerical Estimation of Relative Background Intensity

With the variance defined as above, the value of the background strength relative to that of a source is necessary, as is the value of the CWT. We turn now to the estimation of the relative background, as is performed using the numerical algorithm described in this work. For a source of flux S ($photons \cdot s^{-1}cm^{-2}$), and a background of strength b ($photons \cdot s^{-1}cm^{-2}sr^{-1}$), we note that the source strength in the direction of the source ($photons \cdot s^{-1}cm^{-2}sr^{-1}$) can be approximated, considering a roughly gaussian source (see Fig. 4.7). Thus, the source strength can be written $\frac{S}{2\pi\sigma_i}$, and so the relative strength of the source and background (herein denoted r_b) is just:

$$r_b = \frac{2\pi\sigma_i b}{S} \tag{4.72}$$

Thus, each photon will correspond to a different value of r_b. With this measure of relative background, and where the value of the CWT is normalized to N (Eqn. 4.37), we can continue on to compute the significance of resolving a given point source.

4.7.2 Point Source Significance Calculation

We must now note that the quantity we eventually want is the ratio of the measured source counts to the error in that measurement, or N/σ_N. Also, the data we have consists of many individual photon events, though of here as individual measurements of the quantity N. For each such measurement, then:

$$\frac{\sigma_N^2}{N} = 1.28 + 2.37 r_b \tag{4.73}$$

For many measurements of the same quantity N, the inverse variance can be found as:

$$\frac{1}{\sigma_N^2} = \sum_i \frac{1}{\sigma_{N_i}^2} \tag{4.74}$$

$$\sigma_N^2 = \sum_i [1.28 + 2.37 r_{b_i}] \tag{4.75}$$

Since the source can be approximated as a gaussian profile (See Fig. 4.7), we can write the relative background strength as eqn.(4.72), where σ_i is the point-spread characteristic corresponding to photon event i, and B is the background intensity in units of average counts per unit area.

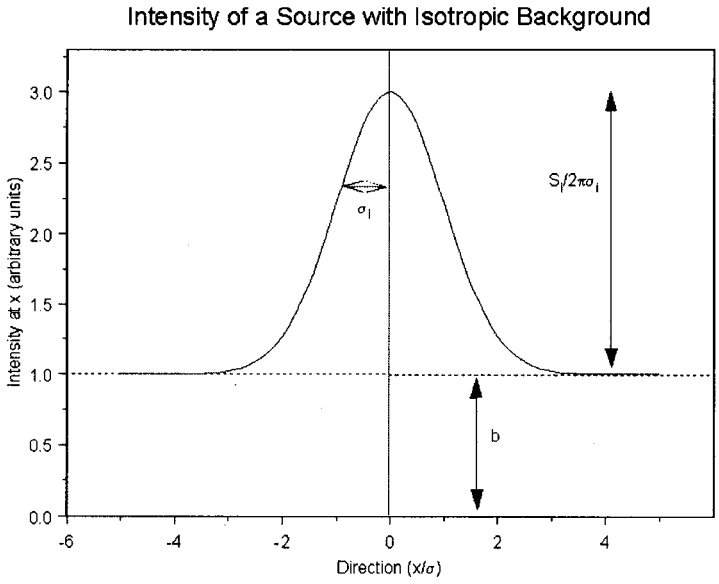

Figure 4.7: Gaussian Source S_i atop diffuse background B

However, we must remember that the sum from 1 to N is intended to identify only counts from a particular source, and since our image is composed of undecided photon events, we must have a method of weighting photons by their probability of belonging to a given source. This is implicitly done in the above sum, as each photon will contain a different contribution to r_b. Thus, with the above calculation performed on the photon map, we can write the remaining estimation of significance, in eqn. 4.75. This estimation for the variance can be seen when a point source is generated using this method, with a given value of r_b, the ratio of background to peak source intensity (see Fig. 4.8). Many identical point sources are created with a background intensity corresponding to the desired value of r_b (in the case of this figure, either 0.0 or 0.5). The MCWT is used to estimate source counts from each

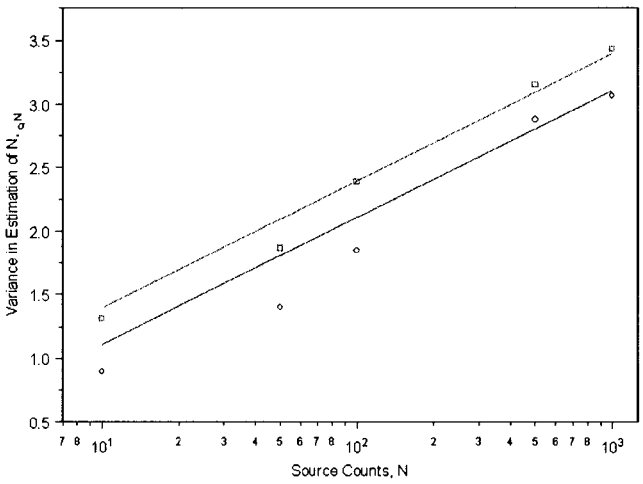

Figure 4.8: Theoretical and actual variances the estimation of a point source for $r_b = 0, 0.5$

identical source, providing an estimate of the variance of counts measurement. This variance is compared to the theoretical calculation.

With an estimated variance on the value of the intensity of a point source at a given location, and with the actual estimated value of that intensity having been set to N for the sake of this calculation, we can conclude that the number of standard deviations from zero the source measurement amounts to, and thus the significance level of the source, is simply the summed inverse variance. Through the use of this method, we can easily set a significance threshold (such as 5σ) at which to estimate point sources.

4.8 Energy Index Estimation

It is worth noting that the property that the normalized multichromatic wavelet transformation has of equaling the number of source counts in the source direction (Eqn. 4.36) can be used to give an estimate of the energy spectrum of a given source. We simply bin all of the incoming photons in our region of interest with respect to energy, and perform the MCWT on each bin, thus giving an estimate of the photon counts came from the source in that bin. As we are mainly concerned with sources emitting power-law spectra, the current implementation of the MCWT algorithm contains a routine to perform this task with constant logarithmic energy bins, as well as to fit the resultant data to a power-law and return the estimated energy index of the source.

4.9 Results

We have produced an analysis of a portion of the sky close to the galactic plane, including the actual sources in the simulated source catalog (circles). (See Fig. 4.9) Here, the x's represent sources that have been reconstructed by the algorithm. In this case, only sources detected to a 4σ significance were considered. The question of source confusion has been addressed by ignoring sources that are separated from each other by less than 1.5 degrees. Given this (and the seemingly good reconstruction of sources in the outlying region), the difficulty of the algorithm of finding sources in regions of high source density is highlighted. See Appendix I for a more complete

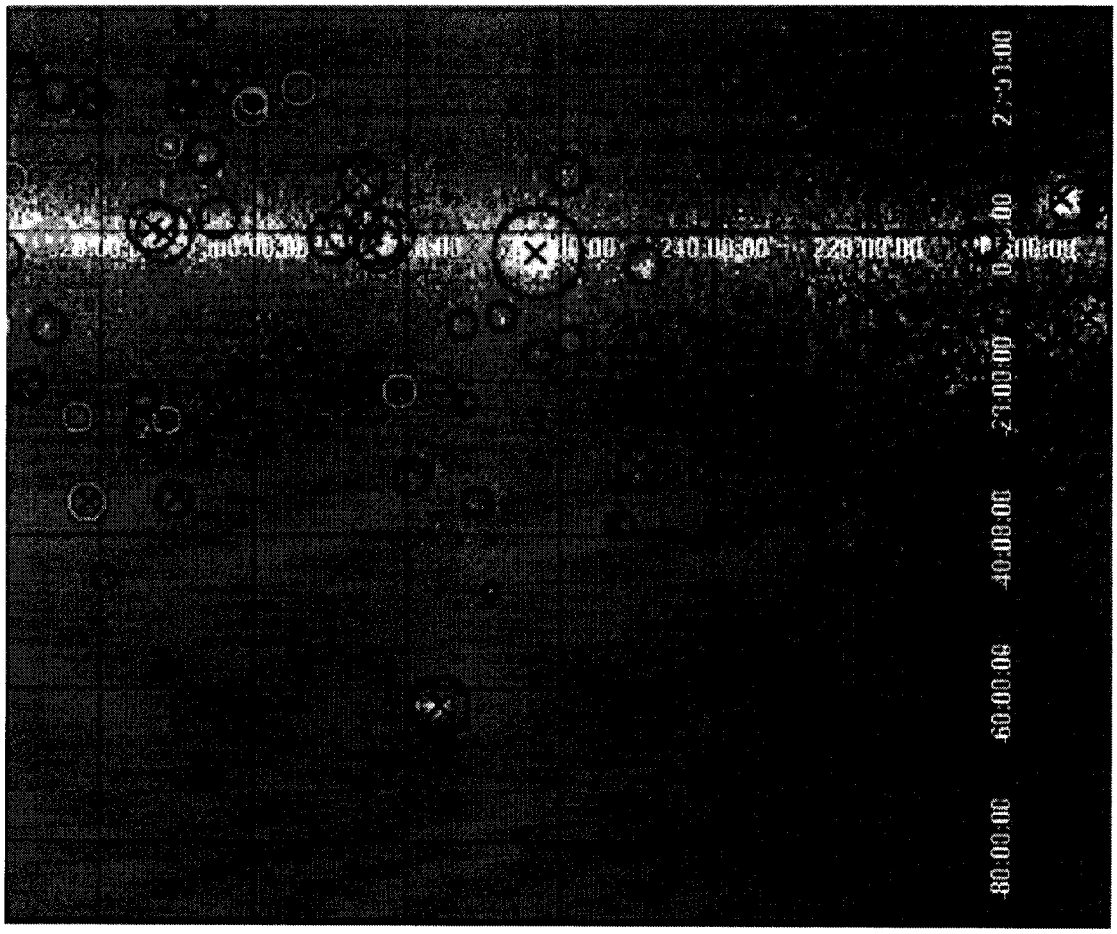

Figure 4.9: Actual and Reconstructed Source Locations

description of the algorithm.

4.10 Alternate Candidate Source Resolution Methods

The wavelet transformation was chosen as a reasonable way to estimate source presences, locations, spectral indices and intensities, largely because it has the capability to do all of these things using the same method. However, a number of source resolution methods have been used and remain in use for resolving potential source from sparse photon data. One of the most famous of these is the method of maximum likelihood, which was one of the methods used to find EGRET sources. Two other methods of interest are aperture photometry and so-called "matched filters," both of which have a similar quality as does the wavelet function; that being the basic nature of a filter function convolved over spatially resolved photons(or, in the case of most binned analysis, a map of pixels representing photon distribution).

4.10.1 Maximum Likelihood(Parameter Gradient Optimization)

Historically, the method described by (Mattox et.al, 1996) has been used to resolve sources from the EGRET data sets. This is an iterative method by which a potential source model is optimized, producing a "best guess" of source parameters. The "likelihood statistic" represents the probability that a given model could have produced the observed data. A model of emission is declared, and this likelihood statistic is calculated. Thereafter, the gradient of the Likelihood in the parameter space al-

lowed is calculated, and the model is shifted in the gradient direction to increase the likelihood. Within some threshold, a local maximum of the likelihood is found.

However, the presence of numerous possible parameters (presence or absence of a source, location of each possible source, intensity and spectra, etc.) makes it difficult to simultaneously optimize a model consisting of an unknown number of sources, or sources with entirely unknown locations. For this reason, the current implementations of the ML optimization method must be given a static model for source locations, or be set to locate more exactly or confirm the presence of a single estimated source. For this reason, there is a great need for a source estimation algorithm which could be used to provide "best guess" information to the ML treatment. The MCWT should be useful in this regard.

4.10.2 Matched Filters

Source location has also been performed by use of the so-called "Matched Filter" (MF) method. A filter function including the Instrument Response Function (IRF) is directly convolved with the 2-dimensional image data. A region around the IRF is designated as negative in the filter function, and used to exclude the background around a source (Vikhlinin et.al, 1995). Though it was believed that the necessary discontinuity in the filter function would lead to "edge effects," particularly in regions of quickly varying background, a direct comparison of the MF and MCWT methods has not been performed.

4.10.3 Aperture Photometry

The concept of Aperture Photometry is simple - an aperture (generally circular) is defined on the sky at any given location, and the photon events within the aperture are counted. The area immediately surrounding the aperture is similarly investigated, to obtain an estimate for the background. Though promising, this method evokes several difficulties with background estimation. "Edge effects" from a varying background become very apparent close to the galactic plane, and there is also the issue of accidentally containing other sources within the region used for background estimation. For these reasons, the determination of an optimal aperture size and shape is a difficult problem.

4.11 Discussion

The Multichromatic Wavelet Transformation (MCWT) allows a relatively fast, flexible method to complete point source searches in sparse incoming particle data. In practice, the multichromatic transformation is performed on each incoming photon individually. As the shape parameter (as well as the effective PSF) varies from one incoming photon to the next, the normalization factor for the wavelet transformation and the coefficients of the variance of source counts will have to be recalculated. However, as these integrals are well-understood, this is readily accomplished in software by calculating them once for a reasonable binning of the available parameters, and then interpolating over the parameter space when they are needed in the algorithm.

Another binned aspect of the implementation of the algorithm is the requirement of a location at which to do the transformation. Obviously, one option is to simply declare a binning structure and evaluate the MCWT in each bin. However, as there are sources expected to be resolved by GLAST which will be separated by less than 1 degree, a sufficiently small binning structure would necessitate a very long numerical processing time. In the current implementation, initial guesses for the location of potential point sources are gained from a tight binning of the sky, followed by a thresholding of incident photon counts, to look for local density maxima. Then, each maximum is the first guess as to a possible source location. After this, the method of gradient ascent is employed to localize the nearest local maximum of the wavelet transformation function. Then, the variance of source counts at each candidate maximum is calculated, giving the significance of measuring a point source at that location. This process is thus essentially entirely continuous, relying on no binning-specific analyses. A future possibility is to use the method of Delaunay triangulation or Voronoi binning (Ramella et. al, 2001) to find local density maxima rather than using pixel-binning. Regardless of the scheme we use for guessing the local density maxima (or even if we were to consider every point in the binned intensity map), the method of gradient ascent seems to be a big aid in finding source locations with greatly improved precision. See Appendix I for a more specific schematic of the algorithms involved in the MCWT.

Chapter 5

Simulation: Putting a Lower Bound on Diffuse Emission

5.1 Specific Measures of Important Detector Characteristics

There are several considerations of the detector and resultant data that we must use in our calculation of the diffuse ratio. As the detector cannot be perfect, we must consider the effective detection area the satellite presents (which will surely vary with energy), the "point-spread" uncertainty in the reconstruction of photon directions, and the exposure of the satellite to a given location on the sky.

5.1.1 Effective Area

GLAST will have a field of view of approximately 2.6 steradians. Beyond this, the detector response to photons falls away sharply, leading us to consider the effective detector area "presented to" the sky at a given angle and energy. The effective area of the detector can be thought of as the rate of photon capture reative to the flux of any given source. In the energy range above 300 MeV, GLAST is required to have a maximum effective area (on-axis) of at least 8000 cm^2 (NASA, 1999). It can also

be thought of as a probability that any given incident particle will be captured, and will depend on both photon energy and direction in this respect. For the purposes of these calculations, the effective area of the detector is considered to be flat within the effective viewing angle of GLAST, particularly considering the gradual "smearing" of the satellite exposure, discussed below.

5.1.2 PSF

As discussed in section 4.6.2, the GLAST Point-Spread Function has been parameterized with respect to a shape parameter, which itself is a function of photon energy and incident angle with respect to the detector. The effective value of the point-spread (taken as a 1σ positional accuracy) is required to be less than 3.5 degrees at 100 MeV, and less than 0.15 degrees above 10 GeV (NASA, 1999).

5.1.3 Satellite Exposure

As GLAST will be orbiting the earth with a period of around 90 minutes, the field of view is "swept" around the sky in a nonuniform fashion. GLAST will operate in a "scanning" mode (where the detector points in some direction relative to the earth zenith, and the orbital motion sweeps the pointing direction around) as opposed to a "pointing" mode (where the satellite would point at a fixed location during orbit). Thus, a pertinent question is the relative exposure of the satellite to any position on the sky. For long observing times(greater than a precessional period), it has been shown (Digel, 2001) that the effective exposure is spread out, achieving flatness to

the level of about $\pm 10\%$.

5.2 Modeling the Emission

5.2.1 Source Model/Spectrum

In concordance with the need for pointlike sources approximating the real estimated distribution, A model representing individual AGN objects is developed, to be added as "point sources" within the greater diffuse emission model. Approximations are made to the nominal energy spectrum index of the sources, as well as their flaring periodicity and modifications to nominal flux and index due to the flaring state. Furthermore, the allowance is made for each of these input parameters to be alterable upon construction of a new AGN-like source. By default, the index of an AGN is around 2.15, while the spectrum hardens by an additional small factor during flaring, and the flux increases by a factor of 5, in accordance with current estimates (Stecker & Salamon, 1996) By default, the software model for the collected diffuse emission will produce and hold many objects corresponding to these AGN sources, the nominal flux of which are calculated randomly, according to the logN/logS characteristic. See Appendix. D for a more complete description of the source generation algorithm.

5.2.2 The "Random" Point Source

To construct a "random" unknown blazar source, we begin by postulating a luminous object with a nominal value of flux ($particles \cdot \sec^{-1} \cdot \mathrm{m}^{-2}$) and energy spectrum (generally a power law at gamma-ray energies), and then allow time-modulations

about these characteristics. See Appendix D for more details about the emission model.

5.2.3 Background Model/Spectrum

The numerical model constituent of the representation of the background is constructed through the GLEAM software architecture. This model allows for the declaration of a logN/logS distribution of sources, from which individual incoming photons are simulated, and allowed to interact with the detector. Thereafter, the incoming photons are reconstructed by the detector through a monte-carlo simulation of the particle interactions afterward (or by a parameterization of those same interactions. This produces the data sets needed for the simulation and estimation of the efficiency of detector resolution, and the estimation of the diffuse ratio (see Appendix. D).

5.2.4 Background Model/Spectrum

In estimating the extragalactic isotropic radiation component, we must be careful to exclude the diffuse emission originating from within our galaxy. Furthermore, in our simulations of the high-latitude emission, we have used the commonly-accepted figure of total isotropic diffuse radiation, around $1.45 \cdot 10^{-5}\mathrm{cm}^{-2}\mathrm{s}^{-1}\mathrm{sr}^{-1}$ above 100 MeV (Sreekumar et.al , 1998). It is important to understand the separation between the isotropic galactic emission and the isotropic extragalactic emission accounted for partially by point sources. The rationale for separating a particular level of the isotropic emission as being extragalactic in nature comes from the presence of two

distinct energy spectra in the total photon emission (Stecker & Salamon, 1996b). It is possible that our estimation of the galactic diffuse emission is low, and some of the truly diffuse "extragalactic" radiation actually originates from within the galaxy (Keshet et.al, 2004). However, if this is the case, more careful estimates of the galactic component will only yield a simple modification to our estimate of the remaining diffuse emission.

5.3 Putting it together - an Algorithm to Determine if Sources have been "Seen"

5.3.1 Naïve Models of Source Resolvability

There are a number of methods by which to estimate the number of sources an experiment will resolve. One of the most basic methods stems from the calculation of the point source sensitivity of the apparatus. The salient question becomes: Can we say that our fit will have "estimated" existing sources above a threshold? If so, then the catalog of generated sources could be simply "cut" below a certain source intensity, and the remaining sources considered "observed". Obviously, this approach is far too naïve, as the calculation of the PSS presupposes an isotropic background, and our calculation particularly is given for the background at high galactic latitude.

Another potential estimation method is to establish the background at close distances to an observed source, and then reclaculate the PSS at each point in space, creating a "resolvability" function with respect to space. Although this establishes a useful estimate of the eventual resolving power, as well at its spatial dependence, it

is fundamentally flawed, thanks to the density of resolvable sources. As the PSF will average a degree or so, we must consider adjacent sources as part of the background obscuring any given point source, as well as the diffuse background. However, until a given source is resolved, its flux has not been measured, and this cannot be considered as the background of an adjacent source. In this way, the PSS estimate will be poor in the limit of many resolvable sources, and we must attempt to simultaneously resolve all of the sources in any given region, as well as the background intensity. Therefore, the method of maximum likelihood provides the best way to estimate source resolution for GLAST.

5.4 Source Confusion and the Falloff of Resolution

We expect to see many sources in the actual GLAST data (Sec. 6.1), as well as a highly anisotropic diffuse radiation component from the galactic plane. Analytical calculations of the Point Source Sensitivity of GLAST have largely relied on the spatial isolation of the sources involved, and are also considering sources in regions of high-latitude (Appdx. A). The complex relation of source density with resolving power of a source estimation model makes an analytical treatment of the actual PSS difficult, particularly as the number of expected sources grows large and the assumption that sources are spatially removed from one another cannot apply. We expect some amount of source confusion, where the model will either resolve two close sources as only one, or perhaps resolve neither. There is also the possibility of being unable to resolve a dim source in the immediate vicinity of a brighter one.

For these reasons, the actual resolution efficiency of any method we choose to use is more easily approximated numerically, by producing a simulated catalog of sources and estimating their resultant data(See Fig. 4.6). In the following sections, then, the efficiency of the algorithm in resolving sources at a given intensity is understood to be calculated numerically by this method.

5.5 Finding the True-Diffuse Ratio

A central point of this paper is the estimation of the contribution of truly diffuse extragalactic intensity to the entire observed extragalactic flux. Several approaches have been considered to accomplish this task, and we will briefly review them.

5.5.1 Intensity Integral Extrapolation

One way to estimate the Diffuse Ratio is to directly subtract the summed AGN emission component from the total extragalactic flux. We consider the integral intensity above any given intensity:

$$S_{int} = \int_{S_{min}}^{\infty} S\frac{dN}{dS}dS \tag{5.1}$$

See fig. 5.1. Making this intensity integral calculation has been done before to estimate the AGN contribution to the total intensity (Chiang et.al, 1995). Finding the relative intensity between the AGN sources and the remaining flux, we calculate the Diffuse Ratio:

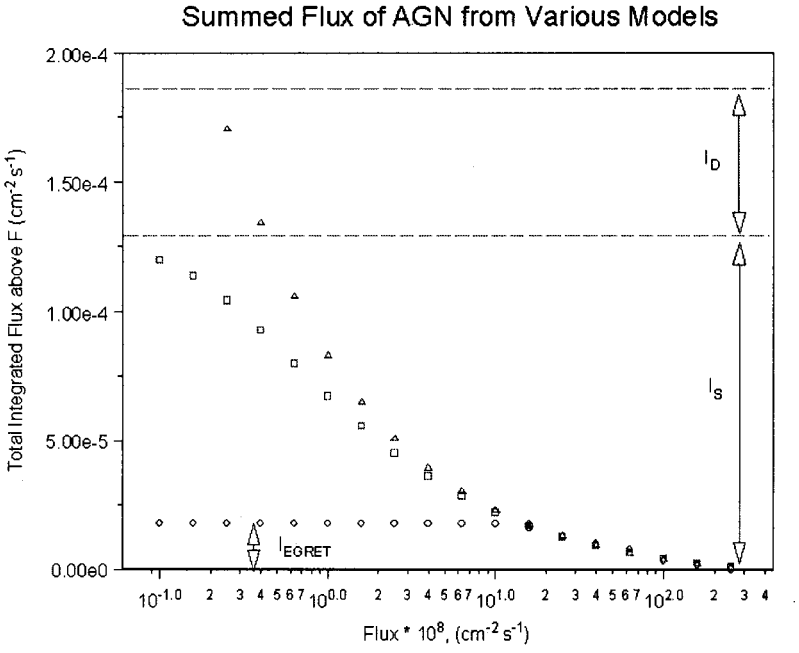

Figure 5.1: Cumulative Intensity Above a flux S, for various AGN catalogs (simulated and EGRET). Circles are EGRET Source Catalog, Triangles are from the (3/2) Power-Law Approximation, Squares are from a Catalog with Arbitrary Negative Density and Luminosity Evolution.

$$D = \frac{I_D}{I_S + I_D} = \frac{I_D}{I_{tot}} \tag{5.2}$$

The logN/logS curve below the EGRET sensitivity threshold must be approximated, and the asymptotic behavior of the curve gives the proportion of the total flux accounted for by the AGN. The combined EGRET catalog flux is found to be about $1.8 \cdot 10^{-5}\mathrm{cm}^{-2}\mathrm{s}^{-1}$. Thus, an upper limit on D is already given by EGRET:

$$D_{UL} = \frac{I_{tot} - I_{EGRET}}{I_{tot}} = 0.889 \tag{5.3}$$

By this reasoning, we can assume that the diffuse intensity can account for no more than 89% of the sky. The lower GLAST sensitivity should help to put a much stronger constraint on this level. However, as mentioned in section 2.3.1, as the density evolution of sources is not well characterized, finding an uncertainty in D as estimated by this method is difficult.

5.5.2 logN Ratio Test

As we have mentioned before, the total Gamma-ray emission of the sky in the range above 100 MeV has been found to be $((1.45 \pm 0.05) \cdot 10^{-5}\ photons\ cm^{-2}\ s^{-1}\ sr^{-1})$, with a power law of about (2.10 ± 0.03) (Sreekumar et.al , 1998). With knowledge of the galactic foreground emission, we can use our reconstruction of logN/logS to estimate the diffuse intensity of the sky. Starting from the assertion that the sum of the logN/logS curve and the extragalactic diffuse emission must equal the total

intensity not accounted for by the galactic emission:

$$Tot.Int. = Galactic\ Foreground + EDGRB + \frac{1}{4\pi}\int (dN/dS) \cdot S \cdot dS \qquad (5.4)$$

we note that a good measurement of logN/logS enables us to estimate the Diffuse Ratio D:

$$D \equiv \frac{EDGRB}{Tot.Int. - Galactic\ Foreground} \qquad (5.5)$$

Thus, if we were to impose $r_b = 0$ (the case of no diffuse intensity), we would expect a curve corresponding to the predicted $logN/LogS$ of Fig.2.3. However, if $r_b > 0$, we expect a depressed curve. Specifically, as any diffuse extragalactic source extends throughout the same space as contains luminous sources, we expect that any given spherical shell extending from radius R to R+dR will have only $1 - r_b$ times the expected number of sources in that area for $r_b = 0$, as the remaining intensity is then accounted for by diffuse flux (Fig. 5.1). Thus, we expect that we can write a point source luminosity function and a diffuse luminosity function, which sum to the entire GLF.

Thus, we expect the number of sources at any intensity to fall with the instrument sensitivity, resulting in an expected falloff at low intensity (Fig. 5.2). Furthermore, the expected value of the logN/logS curve at every intensity yields a measurement of the value of the Diffuse Ratio.

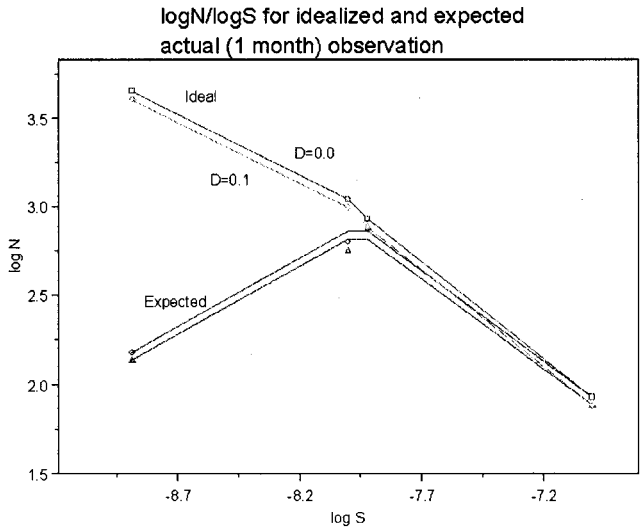

Figure 5.2: Expected logN/logS for $r = 0, 0.1$ - Theoretical logN/LogS curves for a perfect instrument, and actual simulated curves, including PSS/sensitivity falloff.

5.5.3 Measuring the Diffuse Ratio with the logN Ratio Test

Neglecting uncertainties for the moment, we would find the actual N/LogS curve by simply dividing the reconstructed N/LogS by the calculated efficiency of the method at each intensity. The diffuse ratio can then be calculated by using the ratio of the calculated N to the expected N for r=0. So, for each intensity bin I, we have a number of actual (simulated) sources $A(I)$, a reconstructed number of binned sources $S(I)$, and the total number of sources which would constitute the entire background, $C(I)$. We begin by calculating the ratio of the actual to reconstructed sources:

$$\frac{actual}{reconstructed} \equiv P^{-1}(I) \Rightarrow P(I) = \frac{S(I)}{A(I)} \tag{5.6}$$

Given that each source has some probability of being resolved at its given intensity,

we can assume:

$$\sigma_s = \sqrt{S(I)} \Rightarrow \sigma_P = \frac{\sqrt{S(I)}}{A(I)} \tag{5.7}$$

Then, we note that the diffuse ratio D (the proportion of the sky intensity constituted by point sources) can be found as the ratio of A and C:

$$D(I) = \frac{A(I)}{C(I)} = \frac{S(I)}{C(I)P(I)} \tag{5.8}$$

Thus, each intensity bin gives a measurement of the actual ratio D. We can combine the measurements of R_i in order to get a best estimate for the diffuse ratio R.

5.5.4 Uncertainty in the Diffuse Ratio

Obviously, the above method gives an insignificant calculation of the Diffuse Ratio below some intensity threshold, where the efficiency of the method drops toward zero. Thus, we must consider the uncertainty of a measurement of the diffuse ratio at a given intensity, and then consider each intensity to give an independent measure of the ratio, and thus add the errors together in a weighted way to achieve the best measure of the actual ratio, together with its uncertainty. There are, therefore, many uncertainties we need to understand: Uncertainty of the measured ratio P, of the reconstructed number S, and of the expected "$D=0$" number C. As mentioned above, $\sigma_P = \frac{\sqrt{S(I)}}{A(I)}$, as the uncertainty in S is simply its root. For the quantity $C(I)$, we must be careful. For the sake of estimation of the method, we have set $C(I)$ to be the number of sources at a given intensity if no background flux is included. Thus, its

uncertainty is functionally zero. One reasonable way to approximate the uncertainty of dimmer source densities is to say:

$$\sigma_c = 0, I \geq 10^{-8.5} cm^{-2} s^{-1} \tag{5.9}$$

and

$$\sigma_c \to \infty, I < 10^{-8.5} cm^{-2} s^{-1} \tag{5.10}$$

Once these uncertainties are known, we can combine them to estimate the uncertainty of the measurements of D. Considering propagation of errors for uncorrelated quantities:

$$z = f(a,b,c) \Rightarrow \sigma_z^2 = (\frac{\partial f}{\partial a})^2 \sigma_a^2 + (\frac{\partial f}{\partial b})^2 \sigma_b^2 + (\frac{\partial f}{\partial c})^2 \sigma_c^2 \tag{5.11}$$

we then find the variance of the measurement of $D(I)$ at I to be:

$$\sigma_{D(I)}^2 = S(I) \frac{1}{C^2(I) P^2(I)} + \sigma_P^2 \frac{S^2(I)}{C(^2I) P^4(I)} \tag{5.12}$$

And then we combine the measurements of $D(I)$ in the following way: We take the weighted mean of the measurements:

$$\overline{D} = \frac{\sum_i W_i D_i}{\sum_i W_i} \tag{5.13}$$

where $W_i = \frac{1}{\sigma_{D_i}^2}$. Using the weighted mean, the variance of the measurement of D is:

$$\sigma_{\overline{D}}^2 = \frac{\sum_i W_i^2 \sigma_{D_i}^2}{[\sum_i W_i]^2} \tag{5.14}$$

5.5.5 Estimation of D

So, experimentally, the estimation of the quantity D is done thusly: For a known(simulated) $A(I)$, reconstruct sources $S(I)$ with the method, and compute:

$$P(I) = \frac{S(I)}{A(I)}, \sigma_P = \frac{\sqrt{S(I)}}{A(I)} \tag{5.15}$$

Given $C(I)$, for actual sources, reconstruct $S(I)$ and compute:

$$D(I) = \frac{S(I)}{C(I)P(I)}, \ \sigma_{D(I)} = [\frac{D^2(I)}{S(I)} + \sigma_P^2 \frac{D^2(I)}{P^2(I)}]^{1/2} \tag{5.16}$$

We then estimate $\overline{D}$ by combining the independent measurements:

$$\overline{D} = \frac{\sum_i W_i D_i}{\sum_i W_i}, W_i = \frac{1}{\sigma_{D_i}^2} \tag{5.17}$$

And finally the uncertainty in that measurement:

$$\sigma_{\overline{D}}^2 = \frac{\sum_i W_i^2 \sigma_{D_i}^2}{[\sum_i W_i]^2} \tag{5.18}$$

In this way, we can use knowledge of the efficiency of the method, the net unresolved extragalactic isotropic emission, and after having used the method to estimate a log N/log S curve, we are given an estimate for the actual diffuse ratio, and also a method by which to estimate the significance of this measurement. Thus, we can determine

(by using simulated data) the threshold of D at which GLAST will significantly measure a nonzero diffuse extragalactic component.

Chapter 6

Results

6.1 A Simulated logN/logS for GLAST

An important result is the simulated logN/logS relation for GLAST over the course of one year We expect the data line to closely follow the predicted line, up to the instrumental cutoff, as was the case for the EGRET logN/logS (Fig. 2.3). Using our apparatus for source generation and reconstruction (appendix D), and the logN/logS curve estimated in section 2.3.1, we generate sources and high-latitude galactic background for the period of one year, and characterize the resultant estimated source catalog in the same way as was done for EGRET, by plotting the logN/logS curve (Fig. 6.1). We use the approximation of an EGRB constituted by AGN sources (D=0), and consider the GLAST PSF function explained in section 4.6.2. In this analysis, only photons converting within the 12 "thin" conversion planes at the front of the detector were considered, as opposed to the 4 thick layers. By this process, 2673 sources were reconstructed from the simulated data, and 2673 were at most 1.0 degrees away from actual simulated sources. Thus, we expect a source catalog compiled after one year to contain around 2673 sources, using this method. Note

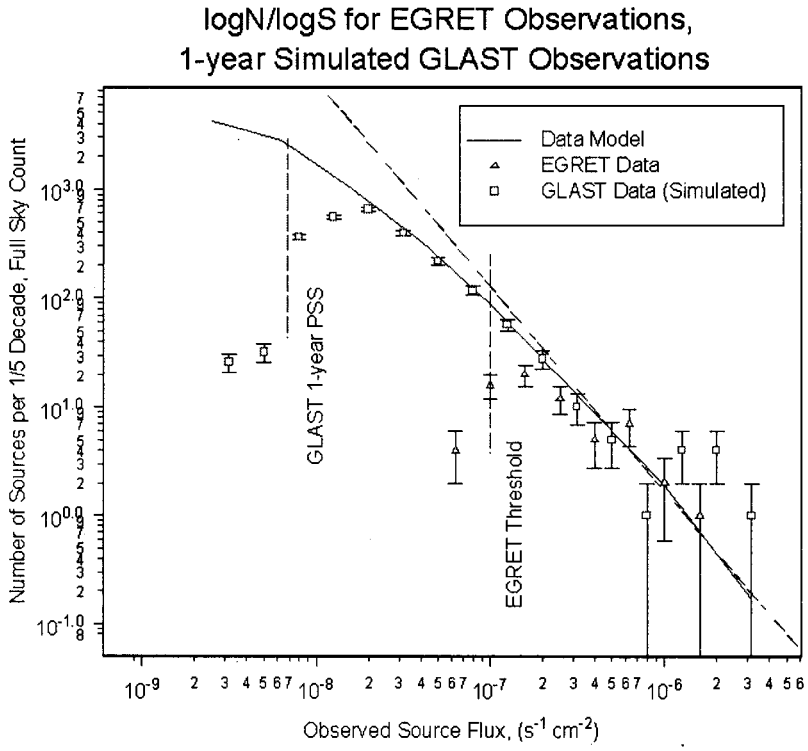

Figure 6.1: logN/logS for a one-year simulated GLAST observation, EGRET data. Data points are resolved sources.

the falloff of effective resolution shown prominently in the figure. We can graphically estimate the one-year PSS for GLAST, using this source resolution scheme, by matching the efficiency falloff of the EGRET source measurements. We calculate approximately $7.0 \cdot 10^{-9}$ cm^{-2}s^{-1}, a bit higher than the PSS estimated assuming well isolated sources.

6.1.1 EGRET data and GLAST data as upper limits on the Diffuse Ratio

As mentioned in section 5.5.1, we can use the EGRET detected AGN catalog to set an absolute upper limit on the contribution of truly diffuse extragalactic radiation

to the sky, about 89%, or $D \leq 0.89$. Although this limit is rather large, it is still useful to note that the EGRET results are inconsistent with a value of D above this threshold. By this same set of reasoning, we can assume that, given some reasonably smooth density and luminosity evolution, as has been estimated by multiple models (Stecker & Salamon, 1996; Chiang ,Mukherjee, 1998), we can expect a cumulative intensity from the GLAST point source catalog to be at least $1.2 \cdot 10^{-4}$. We can thus use Eqn. 5.2 to put a threshold on D of around $\frac{1.8 \cdot 10^{-4} - 1.2 \cdot 10^{-4}}{1.8 \cdot 10^{-4}} = 0.3333$. For this reason, in rigorous evaluation of the diffuse ratio, we consider values of D below this limit.

6.2 Diffuse Discrimination Threshold of GLAST

Much thought has been given to the estimation of the Diffuse Ratio in simulated data. At some value of this ratio, GLAST will be able to significantly resolve it, that is, to find it to be nonzero and significant. As it has been postulated that the ratio may be vanishingly small, this limit on GLAST's capability also provides a lower bound to the EDGRB. Thus, it is an important result to be considered.

6.2.1 The Estimated One-Year High-Latitude Extragalactic Diffuse Discrimination Threshold

We complete the estimation of the discrimination threshold for GLAST for the period of one year. This is accomplished by the method delineated in section 5.5.3. Considering sources in the high-latitude region (not separated by great distances), we

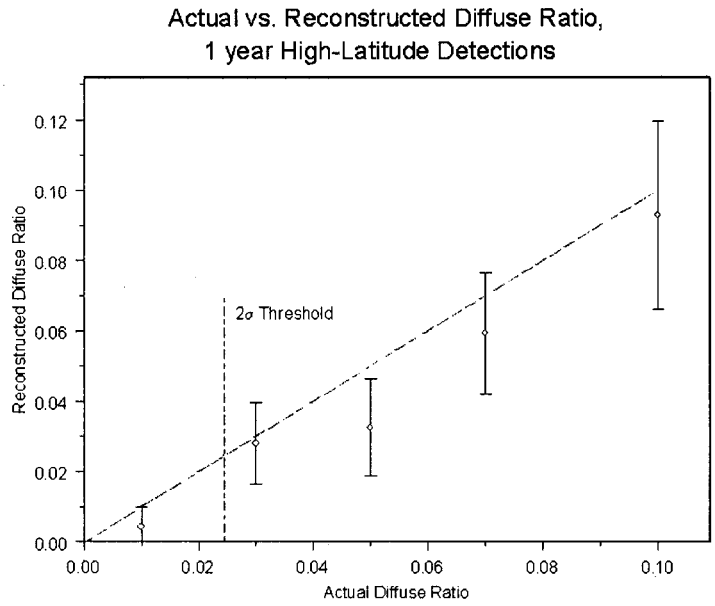

Figure 6.2: Reconstructed Diffuse Ratio for a one-year simulated observation.

create data sets corresponding to values of the diffuse ratio D, and then reconstruct D using the Multichromatic Wavelet Transformation method and the source resolution infrastructure developed in this work(Sec. 5.5.1). The resulting resolution of D is quite good for one year (Fig. 6.2). We attempt to determine the value of D necessary to be measured with a significance of 2σ. By this analysis, GLAST should be able to resolve a component of the total extragalactic radiation from diffuse emission at the level of about 2.5% of the total EGRB, or around $3.625 \cdot 10^{-6}$ $\mathrm{cm}^{-2}\mathrm{s}^{-1}\mathrm{sr}^{-1}$ above 100 MeV. If no significant diffuse component is found, we may consider this figure as an upper bound on the diffuse extragalactic emission.

6.3 Usefulness of the Multichromatic Wavelet Method

The MCWT has several advantages in implementation over other competing schemes. It allows for a good estimate of source locations (and a rigorous development of the source significance to facilitate threshold setting. This is accomplished with an arbitrary number of sources, and there is no real need to find original positions of sources and then estimate further parameters, as there is in the current maximum likelihood implementation, as the locations of individual sources are found via an iterative, nonbinned process. In this way, it is capable of producing results similar to other non-ML methods in use. However, the MCWT also gives an estimate of the intensity, and also the energetic spectrum of the source (within energy binning considerations). This is something which had not yet been accomplished outside of the entire Maximum Likelihood treatment, and thus the method stands as a useful way to fully characterize potential sources.

6.4 Conclusions

This work represents one of the first numerical analyses of the number and intensity threshold of AGN detections made by GLAST over the first year. The method considers numerically the effects of source confusion and the sensitivity falloff of a point source resolution method, in addition to the relation of detector sensitivity to the relative background. The number of expected AGN detections via the MCWT (around 3600) is about 40% of what has been calculated assuming a 5σ threshold of

$1.5 \cdot 10^{-9}\text{cm}^{-2}\text{s}^{-1}$ above 100 MeV (Chen et.al, 2004).

We have established that the multichromatic wavelet transformation has a useful role as a point-source resolution and characterization tool, with several advantages over other numerical algorithms which either resolve only position or other salient source characteristics. In a single analysis, the MCWT is able to estimate location, intensity, spectral index, and significance values for an arbitrary number of sources over an area of interest. By use of this method together with statistical reasoning, we can deduce that the GLAST experiment will be capable of putting a very small lower-bound on the level of extragalactic diffuse radiation present in the region above 100 MeV. Specifically, GLAST should be able to resolve a diffuse component from the EGRB that is as little as 2.5% of the total, or to set a lower bound at 2.5% if no diffuse component is found. This sets a limit of resolvability on the actual diffuse EGRB at $3.625 \cdot 10^{-6}$ $\text{cm}^{-2}\text{s}^{-1}\text{sr}^{-1}$ above 100 MeV.

Furthermore, an immediately useful result of this work has been the characterization of the GLAST Point Source Sensitivity as found when using the multichromatic wavelet transformation method of source location. Using this numerical algorithm, the PSS over 1 year is estimated at $7.0 \cdot 10^{-9}\text{cm}^{-2}\text{s}^{-1}$. The analysis tools developed herein should be of use to the GLAST collaboration and others in analyzing GLAST data once it is available.

Bibliography

The American Physical Society, *Physical Review D: Particles and Fields, Part I: Review of Particle Physics*, American Institute of Physics (July 1, 2002)

Markus Boettcher, James Chiang, Ap.J. 581,127-142 (2002)

Burnett, T., 2004,
http://www-glast.slac.stanford.edu/software/AnaGroup/PSF_analysis.pdf

Chen,A. ,Reyes,L. ,Ritz,S. , AIP Conf.Proc.510:759-763(2004)

Chiang et.al, ApJ 452,156(1995)

Chiang,J., & Mukherjee, R. ApJ 496:752 (1998)

Cowan, G. *Statistical Data Analysis*, Oxford Science Publications, Clarendon Press, Oxford (1998)

Damiani, F. et.al, A Method Based on Wavelet Transforms for Source Detection in Photon-Counting Detector Images (I, II), Ap.J 483:(350-369,370-389), July 1, 1997.

Damiani,F, et.al, A Source Detection Method for ROSAT/PSPC X-Ray Images based

on Wavelet Transforms, Astro. Data Analysis Software and Systems V, ASP Conference series, Vol.101, 1996

Arnon Dar, Nir J. Shaviv, Phys.Rev.Lett.75:3052-3055 (1995)

Digel, S. Talk given at the GLAST Science Working Group Meeting, http://glast.gsfc.nasa.gov/science/swg/apr01/SDigel.pdf (Apr. 2001)

P. Sreekumar et al.,*EGRET Observations of the Extragalactic Gamma-Ray Emission*, Ap.J. 494:523-534 (1998)

Fichtel,Simpson, Thompson, ApJ 222,833 (1978)

Gehrels, N., Michelson, P.,*GLAST: The Next-Generation High-Energy Gamma-Ray Astronomy Mission*,Astroparticle Physics 11:1-2,277-282 (June 1999)

Johnson, Neil, LAT calorimeter subsystem preliminary design report (http://hese.nrl.navy.mil/glast/CALPDR/Cal_PDR_Presentations.pdf). Document #LAT-TD-00242-D6

Jones, T.W., O'Dell, S.L., & Stein, W.A. ApJ 188:353, 1974

Keshet U., Waxman E., Loeb, A.,*The case for a low extragalactic gamma-ray background*, J. Cosmol. Astropart. Phys. JCAP 04(2004)006

Kino, M., Takahara, F., & Kusunose, M., *Energetics of TeV Blazars and Physical Constraints on Their Emission Regions*, ApJ 564:97-107, 2002

J.G.Kirk, F.M.Rieger, A.Mastichiadis, Astron.Astrophys.333:452-458 (1998)

Lachieze-Rey, Marc & Gunzig, Edgard, The Cosmological Background Radiation, Cambridge University Press, 1999.

Lin et.al, 1999, http://arxiv.org/PS_cache/astro-ph/pdf/9905/9905145.pdf

Mattox et.al, The Likelihood Analysis of EGRET Data , Astrophysical Journal v.461, p.396, (1996)

Mattox et.al, ApJ 481,95 (1997)

Mukherjee and Chiang, AstroPart.Phys 11,213-215 (1999)

Nandra, K. *X-Ray Variability of AGN and Correlations with Special Properties* arXiv:astro-ph/0012448 v1 20 (Dec 2000)

Gamma-ray Large Area Space Telescope (GLAST) Science Requirements Document - Final (July 9, 1999) (http://glast.gsfc.nasa.gov/science/resources/aosrd/)

Nemiroff,R.J., Norris , J.P., Bonnell,J.T., Scargle,J.D. Proceedings of the 3rd Huntsville Symposium on Gamma Ray Bursts, Huntsville, AL, 25-27 Oct, 1995. In *Huntsville 1995, Gamma-ray bursts*, vol. 1,507-511 (1995). (e-Print Archive: astro-ph/9602007).

Ormes et. al, Anti-Coincidence Requirements and Implications for the GLAST Trigger and Rates. (http://lhea-glast.gsfc.nasa.gov/acd/ddss/ACD.pdf).

Rachen, Joorg P, *Hadronic blazar models and correlated X-ray/TeV flares*, Published in Snowbird 1999, Towards a Major Atmospheric Cherenkov Detector", 41-52

Ramella et. al, 2001, http://www.arxiv.org/PS_cache/astro-ph/pdf/0101/0101411.pdf

Ressell, M. T. & Turner, M. S., Comm. on Astrophys., 14:323. (1990)

Sambruna, Rita M, *Understanding Blazar Jets Through Their Multifrequency Emission*, Published in Snowbird 1999, Towards a Major Atmospheric Cherenkov Detector, 19-30.

Starck, J-L, Murtaugh, F, and Bijaoui, A, Multiresolution and Astronomical Image Processing, ASP Conference Series, 77, 1995

Stecker, F.W., Salamon, M.H., The Gamma-ray Background from Blazars: A New Look, ApJ 464:600-605, 1996 June 20.

Stecker, F.W., Salamon, M.H., *Comment on the Origin of the High Energy Diffuse Gamma Ray Background* Phys.Rev.Lett. 76:20, 3878 (1996)

Stecker, F.W., Salamon, M.H., *The Extragalactic Gamma-Ray Background* arXiv:astro-ph/0104368 v1 23 Apr 2001

Taylor, John R., An introduction to Error Analysis, University Science Books, 1982 (1997)

Terrier, R. et.al, Wavelet Analysis of Egret Data, Proc. ICRC 2001:Copernicus Gesellschaft 2001.

D. Tsiklauri, V.M. Nakariakov, A three dimensional magnetohydrodynamic pulse in a transversely inhomogeneous medium.Astron.Astrophys.393:321-329,2002

Vikhlinin,A., Forman,W., Jones,C., Murray,S. *Matched Filter Source Detection Applied to the ROSAT PSPC and the Determination of the Number-Flux Relation* Ap.J 451,542 (1995).

Appendix A

Appendix A - Calculation of the GLAST Point Source Sensitivity (PSS)

We would like to make an estimate of the intensity S ($s^{-1}cm^{-2}$) that an isolated point source would need to have in order to be resolved to a significance of 5σ. We use the idealized situation of a wavelet transformation of a point source which is far away from any other sources. Beginning with the inverse variance of the CWT estimation of source counts from a source with relative background density $r_b = \frac{2\pi\sigma b}{S}$:

$$\sigma^{-2} = \frac{1}{N(A + Br_b)} \tag{A.1}$$

where A and B are the coefficients from the integral in Eqn. 4.55. We consider the inverse variance to be the probability that a particular photon contributes to the signal counts in the estimation of the source. Then we consider the approximate total number of source counts from the source and background(within an area $2\pi\sigma^2$) over a time t(sec):

$$C_{tot} = N_{src} + N_{bkg} = t(S(1 + r_b)) \tag{A.2}$$

and the number of source counts needed to achieve a 5σ significance is $5^2 = 25$, which gives us the relation:

$$25 = \sigma^{-2} C_{tot} = (\sigma^{-2}) t (S(1 + r_b)) \tag{A.3}$$

Considering that we have the measures for the high-latitude background and the energy spectrum of an average AGN source, we can write:

$$t = \frac{25}{(\sigma^{-2}(E))(S(E)(1 + r_b(E)))} \tag{A.4}$$

and

$$r_b(E) = \frac{2\pi\sigma(E)b(E)}{S(E)} \tag{A.5}$$

where $\sigma(E)$ is the effective PSF of instrument resolution, $b(E)$ is the high-latitude galactic diffuse emission, $2 \cdot 10^{-5}(\frac{100MeV}{E})^{1.1}$, and $S(E)$ is the normaized source intensity distribution, $S(E) = S\frac{E^{1.15}}{\int E^{1.2} dE}$. Then, for any source strength S ($s^{-1}cm^{-2}$), we can find the approximate time of resolution by:

$$t = \frac{25}{\int S(E)(r_b(E) + 1)\sigma^{-2}(E)} \tag{A.6}$$

(See Fig. A.1). For one year, this will be about $3 \cdot 10^{-10}(S^{-1}cm^{-2})$. It is important to understand that this estimate can really only be viewed as a lower limit on the possible sources that can be resolved, as actual sources will be in close angular proximity with one another, and will exist even in regions of high and spatially-varying background

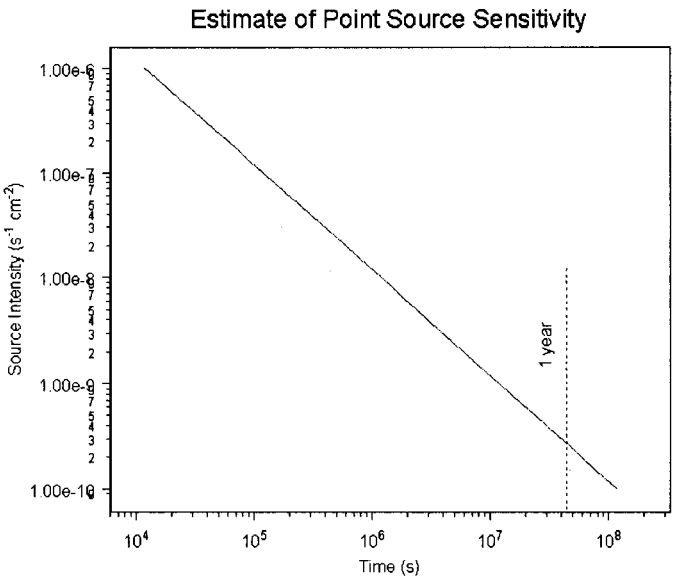

Figure A.1: Calculated Point Source Sensitivity for GLAST (5σ significance)

intensity. Thus, the actual Point Source Sensitivity for any given resolution method is best done by the a careful monte-carlo simulation of the entire emission, as done in section 6.1.

Appendix B

Appendix B - CWT of a Multichromatic Photon Map

We would like to show that the continuous wavelet transform can be shown to be equal to the summation of the Analyzing Wavelet Function evaluated at each point. We accomplish this by performing the binned wavelet transform in the limit of infinitesimal bins. We begin with the definition of the CWT:

$$W_I(\mathbf{b}, a) = \int d^2\mathbf{x}\psi(\mathbf{x}, a)I(\mathbf{x}, a) \tag{B.1}$$

And then consider the binned transformation:

$$W_I(\mathbf{b}, a) = \sum_{i,j} \psi_{ij}(x_{ij}, a)I(x_{ij}, a) \tag{B.2}$$

Note that, for a binned histogram map containing counts, that in the limit of infinitesimal bins, the value of I will be either 0 or 1, as the bins can continue to shrink until no single bin will contain more than one photon count. This is identical to rewriting the image itself as the sum of the individual counts:

$$I(\mathbf{x}) = \sum_i \delta(\mathbf{x} - \mathbf{x}_i) \tag{B.3}$$

And, upon substituting this image into the CWT, we can see that the delta functions eliminate the integral to leave the sum:

$$W_I(\mathbf{b}, a) = \sum_i (\delta(\mathbf{x} - \mathbf{x}_i)\psi(\mathbf{x}, a_i)) = \sum_i (\psi(\mathbf{x}_i, a_i)) \tag{B.4}$$

Thus, the MCWT will be equal to the usual monochromatic CWT if all photon energies are equal, and will have the useful properties of the CWT (estimation of source counts N, exclusion of uniform background).

Appendix C

Appendix C - Optimization of Dilation Factor as a Function of the Effective Point-Spread

Using the Mexican-hat waveform, and postulating a source of gaussian profile:

$$S(r) = \frac{N}{2\pi\sigma_s^2} exp(\frac{-r^2}{2\sigma_s^2}) \tag{C.1}$$

If we furthermore assume a number of total source counts large enough to minimize poisson noise (an assumption made only to establish the optimal relation between a(E) and $\sigma_s(E)$), we can use the continuous expression for the wavelet transform of the image S(x,y):

$$W(\mathbf{x}, a) = \int d\mathbf{x}^2 \psi(\frac{\mathbf{x} - \mathbf{x}'}{a}) S(\mathbf{x}) \tag{C.2}$$

$$W(\mathbf{x}, a) = (\frac{N}{2\pi\sigma_s^2}) \int d\mathbf{x}^2 (2 - frac x^2 a^2) exp(\frac{-x^2}{2(a^2 + \sigma_s^2)}) \tag{C.3}$$

or

$$W(\mathbf{x},a) = \frac{N}{(\sigma_s^2/a^2)^2}(2 - fracx^2a^2 + \sigma_s^2)exp(\frac{-x^2}{2(a^2+\sigma_s^2)}) \tag{C.4}$$

and W will have a maximum at the location of the source, when x=0, so we can write

$$W_{Peak}(a) = \frac{2N}{(1+\frac{\sigma_s^2}{a^2})^2} \tag{C.5}$$

Considering then the function:

$$Y(a) = \frac{W_p(a)}{a} \tag{C.6}$$

which is the value of the wavelet transform "per unit solid angle," we can easily rewrite:

$$Y(a) \propto a(1+\frac{\sigma_s^2}{a^2})^{-2} = (a^{1/2} + \sigma_s^2 a^{-3/2})^{-2} \tag{C.7}$$

so, taking the differential of Y and setting it to zero:

$$Y'(a) = -2(a^{1/2} + \sigma_s^2 a^{-3/2})^{-3}(\frac{a^{1/2}}{2} - \frac{3\sigma_s^2 a^{-5/2}}{2}) = 0 \tag{C.8}$$

then yields:

$$a^{-1/2} = 3\sigma_s^2 a^{-5/2} \Rightarrow a^2 = 3\sigma_s^2 \tag{C.9}$$

or

$$a_{max} = \sqrt{3}\sigma_s \tag{C.10}$$

Putting this value back into the peak wavelet transform immediately yields

$$W_{Peak} = \frac{9}{8} N_{src} \tag{C.11}$$

where N_{src} is the number of counts from the source.

Supplemental calculation: Variance integral for the gaussian source: We define the unbiased estimator function B(x), where, generally,

$$< B >= \int B(x)S(x)dx = \frac{N_s}{N} \tag{C.12}$$

where N is the total number of events, and N_s is the number of counts from the source. Now, generally, for N events, the estimator t(x) is defined:

$$t(x) = \int_i B(x_i) \tag{C.13}$$

and so

$$< B >=< N >< B >= N\frac{N_s}{N} = N_s \tag{C.14}$$

Also, we examine the expectation value of the square of the estimator:

$$< t^2 >=< N >< B^2 > + < (B^2 - B) >< B >^2 \tag{C.15}$$

$$=< N^2 >< B >^2 +N(< B^2 >^2 - < B >^2) \tag{C.16}$$

$$< t^2 >= N(N+1) < B >^2 +N(< B^2 >^2 - < B >^2) = N^2 < B >^2 +N < B^2 > \tag{C.17}$$

And thus, the variance of the measurement is just:

$$< B^2 > - < B >^2 = N < B^2 > \tag{C.18}$$

Now, in our case, the source function is not normalized, and so:

$$\sum_i B(x_i)S(x_i) = N_s \tag{C.19}$$

Therefore, we note that the convolution integral between the source function and the Analyzing wavelet squared yields:

$$\int dx(B(x))^2 S(x) =< B^2 >< N >= N < B^2 >= \sigma^2_{N_s} \tag{C.20}$$

Which is just the variance of our measurement of the source counts. Thus, the above variance calculations are carried out with respect to the number of counts from the source itself.

Appendix D

Appendix D - Details of the Algorithmic Emission Model

The extragalactic and point-source emission are simulated by making data sets corresponding to detector reconstruction. Procedurally, this set of tasks is accomplished by a set of software called GLEAM:
(http://www-glast.slac.stanford.edu/software/gleam/userGuide/default.htm),
which provides a framework for source and satellite simulation. For the purposes of this work, it is necessary to simulate single sources as well as a collection of sources corresponding to logN/logS. A set of code has been developed to perform this latter task, called ExGalflux.

ExGalflux: Individual AGN sources are declared with a galactic direction, as well as inherent (quiescent) flux, and inherent spectral index. Conditions on the flaring state of these point sources are also input, and, as time progresses, the time of the proceeding flaring state is always held as an internal variable, and recalculated when necessary. By default, the AGN's used for the analyses do not flare, as the result of the MCWT method will not change with time variability of the sources observed.

The collected diffuse model holds not only a list of point sources, but also a total flux over the whole sky. It then attempts to fill in the remaining flux by generating point sources according to a logN/logS characteristic.

First, the constructor calls the functions to read in the logN/logS characteristic from data declared in an XML file. Note: this characteristic is in non-differential format (i.e. N is the number of sources with flux equal to or higher than S). Second, the differential logN/logS curve is obtained and integrated over to find the total unresolved (non-diffuse) flux. Third, each time a particle is needed, the event() function searches through the catalog of known sources to determine if a new source is more likely to appear first. Fourth, if a new source is needed, the algorithm integrates over remaining undeclared flux to find the total, then integrates to a random number between 0 and that total. When the desired bin is reached, a single source is subtracted from the remaining flux in the bin and a new source of that flux is declared.

Detector Simulation: For our purposes, the parameterization of the instrument response function is usually used to obtain "uncertain" values for the incoming photon directions. Once a simulated photon is incident upon GLAST, the energy and actual direction are used to generate a random "best guess" direction" for the photon, which is then used as simulated data in the reconstruction and point-source resolution functions.

Appendix E

Appendix E - Details of the MCWT Source Fitting Algorithm

With any input set of multichromatic incoming photon data, the algorithm accomplishes source location and parameter estimation with the following steps:

Location of Density Maxima: The input data is first processed to obtain local photon density maxima. By default, this is accomplished by binning the sky into 1-degree bins and marking each bin as close to a potential source if it has a larger photon count than its neighbors, and is beyond a user-defined threshold.

CWT Maximization: The value of the MCWT and the spatial gradient of the same is calculated at each local density maximum, and Newton's method is employed to iteratively locate the MCWT maximum closest to the beginning location. This maximum is considered as a potentiial source.

Source Parameter Estimation: Each potential source is analyzed as described in this work, and the necessary parameters are calculated, including the positional uncertainty (error circle), the significance of resolving a nonzero source at that location, and the estimated energy index.

Significance/Angular Thresholding: Several further cuts are made on the potential source catalog. First, a user-defined significance threshold is imposed. Second, it is required that every resolved source is separated by a user-defined distance from every other source. Procedurally, if two sources are estimated to be closer than that threshold, only the one with the higher significance is kept. This is designed to reduce multiple resolutions of a single source.

Source Catalog Output: The algorithm then outputs an estimated source catalog (in ASCII format) with the mentioned parameters listed for each source, as well as estimated location.

Appendix F

Appendix F - Variance of the Estimation of Source Counts for a Gaussian Source

For a point source with a background I(**r**), we have found the variance of the measurement of N, made by the CWT method to be as given by equation 4.45:

$$\sigma_N^2 = \int d^2r |\psi(\mathbf{r}, a)|^2 I(\mathbf{r}) \tag{F.1}$$

Now, if we consider a gaussian Point-Spread Function S,(a=3), then

$$I(\mathbf{r}, a) = S(\mathbf{r}) + r_b S(0) \tag{F.2}$$

and

$$\sigma^2_{N_{gaussian,CWT}} = \int d^2\mathbf{r} |\psi(\mathbf{r})|^2 (S(\mathbf{r}) + r_b S(0)) \tag{F.3}$$

Numerically evaluating this for a=3 (the optimal dilation coefficient for a gaussian source), accomplished by the analysis environment Mathematica, yields:

$$\sigma_N^2 = N(1.289 + 2.370\ r_b) \tag{F.4}$$

This calculation allows us to estimate the significance of a gaussian source.

Appendix G

Appendix G - Point Source Intensity Variance

Follows is the calculation of Toby Burnett of the relative variances of the CWT and ML methods in estimating the source counts from a given source. It is shown that wavelets are not much worse for resolving sources than Maximum Lilelihood, for realistic values of the relative background:

Point source resolution for GLAST PSF, Toby Burnett

Our model is a point source in the presence of a uniform background. We characterize the background by a parameter *b*, the ratio of the background density to that of the signal at the point source position, and assume that the PSF is azimuthally symmetric, defining the radial variable *u*=0.5 (*r*/σ)^2, where *r* is the angular deviation and σ a scale parameter, perhaps the projected sigma.

Define functionals that define functions of the *inverse variance* in the relative signal strength, or resolution, per photon, as a function of b, for maximum likelihood and a projection method. F is the PSF function, P the projection function.

$$\mathrm{norm}(F) := \int_0^\infty F(u)\,du$$

$$\mathrm{Res}_{ML}(F,b) := \frac{1}{\mathrm{norm}(F)} \cdot \int_0^\infty \frac{F(u)^2}{F(u) + b \cdot F(0)}\,du$$

Note that for b =0, this becomes 1: for max L you just count the photons. For large b, the integral of the square of the PSF function is a simple characterization of the resolution.

$$\mathrm{Res}_{Proj}(F,P,b) := \frac{\left(\int_0^\infty F(u)\,P(u)\,du\right)^2}{\mathrm{norm}(F) \cdot \int_0^\infty P(u)^2 \cdot (F(u) + b \cdot F(0))\,du}$$

Derivation of this must allow for poisson fluctuations in the number of photons

Now define the functions: a Gaussian PSF (which is a simple exponential with this scaled radial coordinate), the realistic psf determined from the simulations, and a simple projection wavelet

gaussian	$G(u) := \exp(-u)$	the ideal, with σ the projected sigma
empirical PSF	$psf(u,s) := \left(1 + \frac{u}{s}\right)^{-s}$	s is a "shape" parameter. For small x, and s=2, it is the first terms in a power series of a Gaussian
	$F(u) := psf(u,2.0)$	A value of 2 is typical

wavelet projection $w(u,a) := \left(1 - \frac{u}{a}\right) \cdot \exp\left(\frac{-u}{a}\right)$

$P_3(u) := w(u,3)$

$P_5(u) := w(u,5)$

$P_8(u) := w(u,8)$

The wavelet function has one parameter, the relative squared scale factor a, which can be varied to maximize the resolution. we examine three values. a=3 is known to be the optimal for the gaussian case.

Now look at the resolution functions for maximum likelihood, with gaussian and PSF, and a wavelet projection applied to the PSF. $b := 0, 0.05 .. 3$

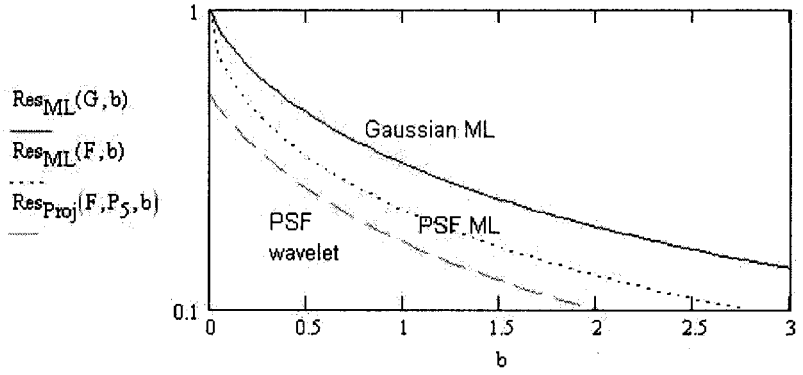

Wavelets are of course not as good as ML, but fairly close. Examine the ratio of ML to projection next

$$\mathrm{Ratio}(F,P,b) := \frac{\mathrm{Res}_{ML}(F,b)}{\mathrm{Res}_{Proj}(F,P,b)}$$

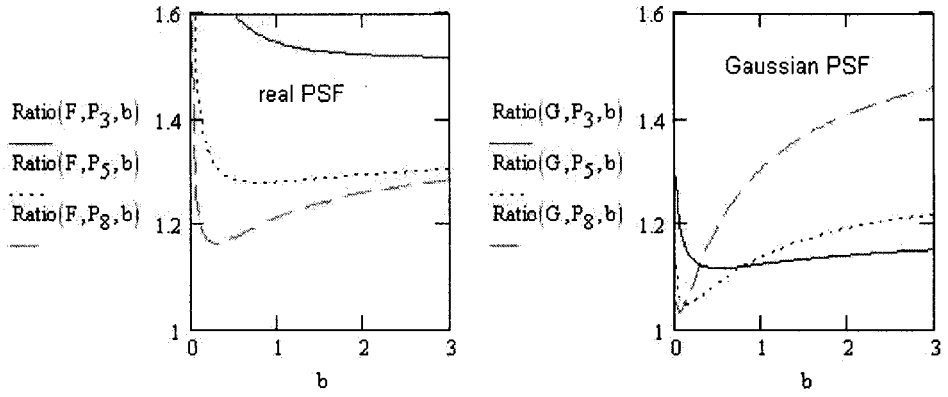

So, never worse than about 30% here.

The estimation of the number of source counts needs to be corrected by the value of this integral.

$$T(F,P) := \frac{\int_0^{\infty} F(u)\,P(u)\,du}{\mathrm{norm}(F)}$$

$T(F,P_3) = 0.287$

$T(F,P_5) = 0.394$

$T(F,P_8) = 0.496$

$T(G,P_3) = 0.563$

Appendix H

Appendix H - Analytical Spatial Resolution

Suppose we want to try to resolve a point source amid a uniform background. There are two relevant questions to be approached at this point: What is the error in spatial resolution, and what are reasonable criteria for us to have declared a source to be "resolved?" For the remainder of this section, I will consider a source located spatially at a position X_0, with a constant rate r, and also a diffuse background, extending to a very large distance (several times larger than the standard deviation of single observations of the point source), with a constant rate R. First, we will consider spatial resolution of a one-dimensional source with no background: Spatially, a source located at X_0 will follow a normal distribution:

$$f(X_0, \sigma_{IRF}) = \frac{1}{\sqrt{2\pi}\sigma_{IRF}} \exp\{\frac{-(x - X_0)^2}{2\sigma_{IRF}^2}\} \tag{H.1}$$

for R=0. Note that f(x) dx is defined as the probability that any given measurement will fall between x and x+dx. The standard deviation of such a normalized gaussian probability density is just σ_{IRF}, physically represented by the instrument response function. We are interested in the Standard Error of the spatial position of

the source, which, after N measurements, is the familiar standard deviation of the mean,

$$\sigma_{\overline{x}} = \frac{\sigma_{IRF}}{\sqrt{N}} \tag{H.2}$$

At this point, it is important to note that we will realistically want to consider sources in two spatial angular dimensions. It is important to note that the two spatial dimensions cannot necessarily be expected to have uncorrelated errors, and so we must carefully examine the source distributions. Assuming for the sake of compact notation that the source exists at the coordinate origin ($X_0 = Y_0 = 0$), we can simply redefine the desired coordinates to be circular polar coordinates, defined by projecting a circle against the sky (θ, ϕ). Noting that $x^2 + y^2 = r^2$, we rewrite the two-dimensional distribution function:

$$F(x,y) = F(x)F(y) = \frac{1}{2\pi\sigma^2} exp(\frac{-\theta^2}{2\sigma^2}) \tag{H.3}$$

and note that $dx \cdot dy = r \cdot dr \cdot d\theta$, so we equate the two distribution functions in terms of their meaning over a unit area:

$$F(x,y)dxdy = G(\theta,\phi)drd\phi \tag{H.4}$$

where G is the distribution function with respect to the polar coordinates, we find

$$G(\theta,\phi) = \frac{\theta}{2\pi\sigma^2} exp\{\frac{-\theta^2}{2\sigma^2}\} \tag{H.5}$$

Integrating over ϕ , we arrive at the radial distribution function:

$$G(\theta) = \frac{\theta}{\sigma^2} exp\{\frac{-\theta^2}{2\sigma^2}\} \tag{H.6}$$

By a similar argument, we can say that the distribution function of θ^2 is

$$G(\theta^2) = \frac{1}{\sigma^2} exp\{\frac{-\theta^2}{2\sigma^2}\} \tag{H.7}$$

As the distribution in θ (and θ^2) is non-gaussian, we must consider the entire distribution in order to establish a confidence contour. Here, we return to the definition of the distribution functions in x and y. As the X and Y measurements will have a gaussian distribution about their "real" values, we can use the method of error propagation in order to define a distribution function of the mean, in the following way. Considering the mean of the measured values of x (each of which has a random error estimated by σ_x), we find that, since

$$x_i = X_0 + \sigma_x, \ and \ \overline{x} = \frac{\sum \sigma_{x_i}}{N} \tag{H.8}$$

we can consider the error in the quantity $N\overline{x}$:

$$\sigma_{N\overline{x}} = \sqrt{\sum (\sigma_{x_i})^2} = \sqrt{N\sigma^2} \tag{H.9}$$

so $\sigma_{\overline{x}} = \frac{\sqrt{N\sigma^2}}{N} = \frac{\sigma}{\sqrt{N}}$.This is the famous "standard deviation of the mean" result. Now, as we know that the estimated values of x and y are also subject to small,

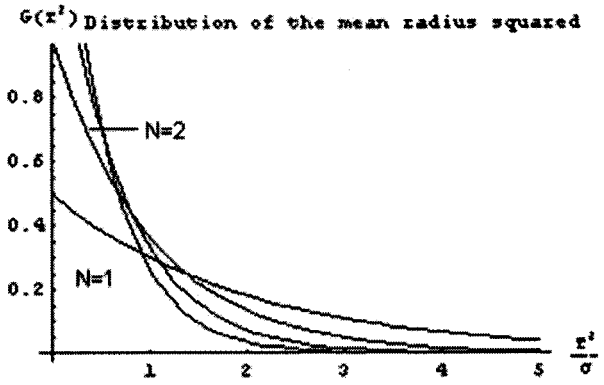

Figure H.1: Distribution of mean radii squared

random errors, we are free to define gaussian distribution functions with the standard deviations of the mean:

$$f(X_0, \sigma_{\overline{x}}) = \frac{1}{\sqrt{2\pi}\sigma_{\overline{x}}} exp\{\frac{(-x - X_0)^2}{2\sigma_{\overline{x}}^2}\} \tag{H.10}$$

(where a similar relation exists for the mean of x), and then find the distribution function for the mean of the quantity r^2 by the same method given above. It is important to note that this will be the same as the result for the distribution functions with respect to r and r^2, except that here we have the condition $\sigma \rightarrow \frac{\sigma}{\sqrt{N}}$. Therefore we can state the normalized distribution function for the mean of r^2:

$$G(\overline{r}^2) = \frac{N}{2\sigma^2} exp \frac{-Nr^2}{2\sigma^2} \tag{H.11}$$

(See Figure H.1). Note that, for N=1, $G(\overline{r}^2) \rightarrow G(r^2)$ With this, we can define the frequentist confidence interval of 95%:

$$0.95 = \frac{N}{2\sigma^2}\int_0^{R_c^2} dr^2 exp\{\frac{-Nr^2}{2\sigma^2}\} = \frac{N}{2\sigma^2}\frac{-2\sigma^2}{N}(exp\{\frac{-NR_c^2}{2\sigma^2}\} - 1) = 1 - exp\{\frac{-NR_c^2}{2\sigma^2}\} \tag{H.12}$$

or

$$\frac{-2\sigma^2}{N} ln(0.05) = R_c^2 \Rightarrow R_c \cong \frac{2.45\sigma}{\sqrt{N}} \tag{H.13}$$

This, then, defines the 95% confidence limit for N measurements of the source location. For nonzero background, however, we must consider a more complicated probability function. This could present a problem, since the probability density is neither flat, nor gaussian. If we can find the deviation of a particular measurement, we can find the standard error of the mean, and thus we would like to know about the statistics of a single measurement. We use the relation from (Taylor, 1997, eqn. 5.16):

$$\sigma_x^2 = \int_{-\infty}^{\infty} (x - \overline{x})^2 f(x) dx \tag{H.14}$$

For the sake of brevity, we can just define $\overline{x} = 0$, as the error, and not the mean, is the desired quantity. So, for a relative background flux of R, we will say that the background flux exists over an effective distance $A_x (A_x \gg 2\sigma)$, so that we can then write f(x) with a gaussian source superimposed on top of a uniform background, with an obvious normalization constant:

$$f(x) = \frac{1}{\sqrt{2\pi}\sigma + A_x R}[exp\{\frac{-x^2}{2\sigma^2}\} + R] \tag{H.15}$$

Invoking Equation H.14, we can see that

$$\sigma_x = \frac{1}{\sqrt{2\pi}\sigma + A_x R} \int_{-\frac{A_x}{2}}^{\frac{A_x}{2}} dx(x^2 R) + x^2 exp\{\frac{-x^2}{2\sigma}\} = \frac{1}{\sqrt{2\pi}\sigma + A_x R}[\frac{A_x^3 R}{12} + \sqrt{2\pi}\sigma^{3/2}] \tag{H.16}$$

At this point, we can write the standard error as:

$$\sigma_{\overline{x}} = \sqrt{\frac{\sigma_x^2}{N}} \tag{H.17}$$

and radially,

$$\sigma_{\overline{r}} = \sqrt{(\frac{\sigma_{\overline{x}}}{\sqrt{N}})^2 + (\frac{\sigma_{\overline{x}}}{\sqrt{N}})^2} = \sqrt{2}\sigma_x \tag{H.18}$$

Taking the case $A_x \rightarrow \infty$, we find that the error in spatial resolution becomes correspondingly large, implying that resolution of a source in an infinite field is an impossible task. This seems somewhat believable, since, as the spatial area available to a single source increases, the probability that random fluctuations will present a given area with enough flux density to imply a source which is not really there, generating an error of the first kind, also increases.

Vita

Sean M. Robinson was born in Portland, Oregon, and grew up in the small town of Aloha, Oregon. He attended Lewis and Clark college, graduating with a Bachelor of Arts degree in Physics and a minor in Mathematics in 1999. He then went on to the University of Washington and earned a Master of Arts Degree in Physics in 2002, followed by a Doctor of Philosophy in Physics in 2004.